Theories of photoelectron correlation in laser-driven multiple atomic ionization

Wilhelm Becker

Max Born Institute for Nonlinear Optics and Short-Pulse Spectroscopy, Max-Born-Strasse 2A, 12489 Berlin, Germany

XiaoJun Liu

State Key Laboratory of Magnetic Resonance and Atomic and Molecular Physics, Wuhan Institute of Physics and Mathematics, Chinese Academy of Sciences, Wuhan 430071, People's Republic of China

Phay Jo Ho

Chemical Physics Division, Argonne National Laboratory, Argonne, Illinois 60439, USA

Joseph H. Eberly

Department of Physics and Astronomy, University of Rochester, 600 Wilson Boulevard, Rochester, New York 14627, USA

(published 17 July 2012)

Experimental advances with laser intensities above 1 TW/cm^2, with pulse durations between roughly 50 and 5 fs, have led to the discovery of new atomic effects that include examples of startlingly high electron correlation. These phenomena have presented an unexpected theoretical challenge as they lie outside the domains of both of the nominally applicable theories, namely, straightforward perturbative radiation theory and quasistatic tunneling theory. The two liberated electrons present a new few-body collective effect. When they are not released independently, one by one, the term nonsequential double ionization has been adopted. Theoretical avenues of attack have emerged in two categories, which are strikingly different. They can be labeled as ''all-at-once'' and ''step-by-step'' approaches. Although different, even conceptually opposite in some ways, both approaches have been successful in confronting substantial parts of the experimental data. These approaches are examined and compared with their results in addressing key experimental data obtained over the past decade.

DOI: 10.1103/RevModPhys.84.1011 PACS numbers: 32.80.Rm, 31.15.V−, 31.15.xg, 32.80.Wr

CONTENTS

I. Introduction to Nonsequential Double Ionization 1011
II. Avenues of Theoretical Study 1013
A. Basic concepts 1013
B. Step by step: Tunneling and recollision 1014
C. Step by step: ''Simpleman'' kinematics 1015
D. All-at-once double-ionization theory 1016
III. Basic Experimental Facts 1017
IV. Description of Theoretical Models 1018
A. Quantum-numerical solutions for helium and other atoms 1018
B. Completely classical trajectories 1020
C. SFA extension via Feynman-diagram modeling 1021
D. Tunneling-classical trajectory methods 1024
V. Comparisons of Theory with Experiment 1026
A. Doubly charged ion-yield measurements: The knee 1026
B. *Ab initio* (TDSE) theory and experiment: Helium 1027
C. Fingerlike structures 1028
D. Recollision–impact-ionization scenario: Neon 1029
E. The species dependence of NSDI 1030
VI. Current Frontiers of NSDI 1032
A. Nonsequential double ionization below the recollision threshold intensity 1032
B. Other wavelengths producing NSDI 1033
C. Strong-field ionization with elliptical polarization 1033
D. Phase-space perspective and classical chaos 1035
E. NSDI of molecules 1035
F. NSDI with few-cycle pulses 1036
G. Nonsequential multiple ionization 1037
VII. Synopsis and Outlook 1038
Acknowledgements 1041
References 1041

I. INTRODUCTION TO NONSEQUENTIAL DOUBLE IONIZATION

Photoelectron dynamics is a fascinating and challenging research topic in atomic and molecular physics. This has been true for more than 100 years. Indeed, Einstein's resolution of the puzzle of the photoelectric effect required him to invent the first quantum treatment of the light-matter interaction (Einstein, 1905). Modern studies of the atomic photoeffect were prompted in the 1960s with the unexpected observation of sparks generated by laser pulses focused in air. The realization that photoionization of air molecules could be produced with optical photons having individual energies far short of the molecular ionization potential was sufficient to initiate optical multiphoton physics as an intriguing research arena.

Since those early observations the light intensity available from pulsed lasers has grown by 10 orders of magnitude,

pulse durations have decreased as far as into the 2–3 cycle range, and pulse repetition rates now reach the megahertz regime. A consequence has been the ability to investigate previously inaccessible multiphoton domains, and a prominent one of these has been the ionization of more than one electron.

An important result, motivating this review, has been the discovery of surprising new phenomena associated with exceptional, even unprecedented, consequences of atomic-electron correlation, signaled by the failure of standard optical ionization theory, well established for one-electron phenomena in high laser fields. This failure can, without undue dramatization, be called catastrophic because the observed double-ionization yields can be 6 or more orders of magnitude greater than the standard theory predicts.

These extremely large double-ionization yields are apparent in Fig. 1, showing experimental data obtained with linearly polarized 100 fs, 780 nm laser pulses as functions of the intensity. Such data are found in a wide range of laser intensities (roughly 10^{13}–10^{16} W/cm^2) with pulses in the 5–50 fs regime. The observed yields cannot be explained by the assumption that electrons are emitted one by one, with the second ionization independent of the previous one. Such a scenario is called "sequential double ionization" (SDI). Therefore, the observed high-field phenomena are grouped under the label nonsequential double (or multiple, meaning triple and higher) ionization or NSDI (NSMI). The term nonsequential still allows that the electrons are emitted in a temporal sequence but implies that the two ionization processes are correlated. NSDI has been observed in all inert-gas atoms from xenon to helium (l'Huillier *et al.*, 1983; Fittinghoff *et al.*, 1992; Kondo *et al.*, 1993; Walker *et al.*, 1994; Talebpour *et al.*, 1997) and in a number of molecules (Talebpour, Larochelle, and Chin, 1997; Cornaggia and Hering, 1998). Similar nonsequential footprints have also been observed in multielectron ionization. The very first observation of nonsequential double ionization occurred earlier for alkaline-earth metals (Aleksakhin, Zapesochnyi, and Suran, 1977).

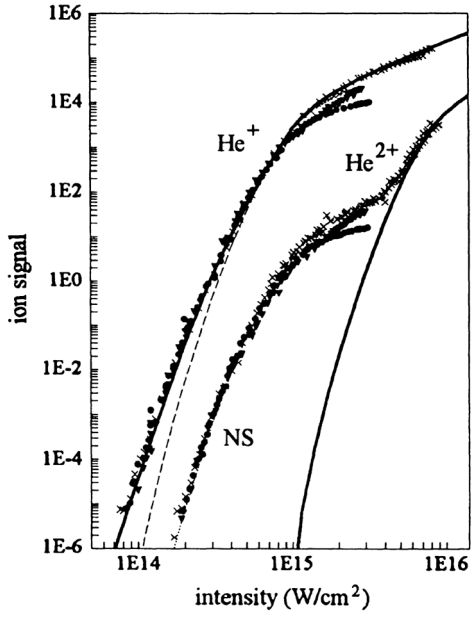

FIG. 1. Dots and crosses show measured total ion yields of He^+ and He^{2+} (the measured intensities are multiplied by 1.15). Solid and dashed lines with the data represent the results of single-active-electron and tunneling calculations. The solid line to the right shows the result expected on the basis of sequential ionization. The experimental results display the NSDI "knee" signature of the ion-count data. From Walker *et al.*, 1994.

The absence of NSDI-type correlation and the return to normal SDI behavior, i.e., ionization of two electrons independently, at intensities exceeding about 4×10^{15} W/cm^2 in Fig. 1 can be loosely attributed to a time lag needed for any high electron-electron correlation to be established. A sufficiently high intensity pulse will remove one or both electrons before correlation can set in. Hence, NSDI is observed only for intensities low enough.

In this overview our interest is to explain and compare the theoretical interpretations that have been developed for the anomalously high He^{2+} counting rates shown in Fig. 1, along with other related phenomena, in a wide array of atoms. The central element of our review is signaled by the choice of the word "interpretations." This is used because for the past 10–15 years the work of both the experimenters and their theoretical counterparts has been mainly phenomenological, that is, a cooperative effort to obtain a reliable semiquantitative understanding of the phenomenology emerging to characterize this new physical domain. Fresh phenomena continue to be predicted and/or observed, and neither calculations nor experimental records have yet reached a level of high precision. Different and in some respects conflicting interpretations of the nature of NSDI effects have been advanced. Remarkably, more than one can be called successful.

Some elements of high-field ionization are built into essentially all theories of both SDI and NSDI and constitute universally accepted approximations:

- So many photons are contained in a typical laser pulse that the effects of field quantization can be safely ignored, so the laser field can be taken as purely classical.
- The typical laser wavelength is so long compared to atomic dimensions that the dipole approximation is completely acceptable, and the electric field can be taken as independent of position, which we indicate in writing it as $\mathbf{E}(t)$.
- Nonrelativistic theory is suitable to capture all aspects identified in experiments to date (except for multiple ionization at intensities exceeding some hundreds PW/cm^2).

All three of these approximations have been adopted generally. They will not be mentioned further. A further assumption, commonly called the single-active electron (SAE) approximation [see Kulander, Schafer, and Krause (1992)], is that core electrons play only static roles in a high-field multi-ionization event. Adapting this to NSDI, SAE implies two independently active electrons, while the inactive core comprises the remaining electrons. Except when we discuss single ionization, it is in this sense that we employ SAE in this review. This is, of course, perfectly justified only in helium,

where there is no core. The majority of experimental results have been obtained for atoms other than helium, and we will see that different theories approach the influence of a static core in different ways.

Two final points rarely mentioned are that (a) in NSDI theories electrons are treated as spinless bosons, and (b) the three-body Coulomb interaction has no known solution. A consequence of the latter is that there is no known way to specify conditions on the two outgoing electrons in NSDI that will guarantee a double ionization. That is, one of the electrons may always return to the core and push the other one away faster. To be more pedantic, there are no known two-electron state vectors that are outgoing and have zero overlap on all bound states. Thus all theories share the need to adopt an arbitrary criterion for ionization. Fortunately a wide variety of "reasonable" specifications, such as sufficiently great energy or distance from the nucleus, all give closely similar results.

Earlier reviews of nonsequential double ionization were given by Dörner *et al.* (2002), several chapters in the book by Ullrich and Shevelko (2003), and also by Becker and Faisal (2005), Becker, Dörner, and Moshammer (2005), and Becker and Rottke (2008). A recent review by Figueira de Morisson Faria and Liu (2011) focuses on quantum-mechanical approaches. We also list some reviews of related topics that may be helpful. Early work on multiphoton ionization is reviewed by Mainfray and Manus (1991) and Delone and Krainov (1998). The theory of laser-atom interaction before the advent of ultrashort pulses has been covered by Faisal (1987), Fedorov (1997), and Joachain, Dörr, and Kylstra (2000).

There are two one-electron high-field effects, high-order harmonic generation (HHG) and high-order above-threshold ionization (ATI), whose mechanisms have much in common with NSDI. They are surveyed by Salières *et al.* (1999), on the one hand, and by DiMauro and Agostini (1995), Becker *et al.* (2002), and Agostini and DiMauro (2008), on the other hand. The transition, for laser-atom processes in general, from the nonrelativistic to the relativistic regime is reviewed by Salamin *et al.* (2006).

II. AVENUES OF THEORETICAL STUDY

A. Basic concepts

High-field ionization theory had its origin in the 1960s with attempts to calculate multiphoton ionization rates for single-electron ejection. The N-photon generalization of Einstein's famous photoelectric equation of energy conservation clearly expresses the reaction to be addressed:

$$N\hbar\omega - I_P = \text{K.E.} + U_P. \tag{1}$$

Here K.E. is the observed drift kinetic energy of the liberated electron and U_P is a new energy term described below. N is the number of photons needed to match or exceed the ionization potential I_P of the atom targets. It is typically in the range 10–15 at optical wavelengths.

The U_P term was not originally associated with the photoelectric effect, but is now significant. It is the cycle-averaged energy of free-electron oscillation in the laser field $\mathbf{E}(t)$ and is referred to as the "ponderomotive energy" (Boot, Self, and Shersby-Harvie, 1958; Kibble, 1966; Eberly, 1969). It is adiabatically returned to the field at the end of a short pulse (now the standard situation), while for an electron leaving a long pulse it is converted into directional kinetic energy (Bucksbaum, Bashkansky, and McIlrath, 1987). It is given by

$$U_P = \frac{e^2\langle \mathbf{E}^2\rangle}{2m\omega^2} = 9.3\times 10^{-20}\lambda^2 I, \tag{2}$$

which evaluates U_P in eV for an atomic electron when λ and I are expressed in nm and W/cm^2. At common NSDI intensities, with I in the range 3×10^{13}–3×10^{15} W/cm^2, the ponderomotive energy will become significant. For a mid-range intensity and the most common laser wavelengths $\lambda \approx 800$ nm, we have $U_P \sim 40$ eV. And for a rare-gas atom ionized by an infrared CO_2 laser (Chin, Yergeau, and Lavigne, 1985), U_P can be large enough to raise the photon number threshold to as much as 10 times the nominal N based on I_P alone.

It was quickly realized that traditional expressions for ionization rates are essentially useless in the multiphoton domain of interest for two reasons. The first reason is that the radiative interaction is not weak for the laser intensities employed, making perturbative convergence nontrivial. For reference, the effective coupling constant is not $\alpha \simeq 1/137$ but the much larger dimensionless ratio that appears N times in an Nth-order bound-state perturbation calculation. This is the not-small quantity

$$\left|\frac{\mathbf{d}_{ij}\cdot\mathbf{E}(t)}{\hbar(\omega_{ij}-\omega)}\right| \approx 1.7, \tag{3}$$

where we have used ea_0 to estimate $|\mathbf{d}_{ij}|$ and have taken an "average" energy mismatch to be $\frac{1}{2}$ eV, and have used a laser intensity of 10^{14} W/cm^2 to calculate the cycle-averaged magnitude of $\mathbf{E}(t)$.

The second reason is sheer calculational complexity; given the vast number of angular momentum channels available, the number of intermediate states required to be included in even a lowest-order calculation is completely impractical when more than five laser photons (and more than 20 in some atoms) are required to reach the continuum final state from the ground state. Early partial-summation theories and other systematic methods designed to avoid order-by-order calculation did not achieve useful results (Bebb and Gold, 1966; Gontier and Trahin, 1989), so a different theoretical treatment was needed. In the following sections, we introduce the few that have been most highly developed to date.

Every theoretical approach must recognize five relevant NSDI interactions, all strong and roughly equal in importance: two interactions of the laser field with the two electrons, and three Coulomb interactions—both electrons with the doubly charged ion, and the two electrons with each other. If we fix the nucleus to the origin of our coordinate system, the two-electron Hamiltonian is

$$H = \frac{\mathbf{p}_1^2}{2m} + \frac{\mathbf{p}_2^2}{2m} + V_{n,1}(r_1) + V_{n,2}(r_2) + V_{ee}(r_{12}) - e(\mathbf{r}_1+\mathbf{r}_2)\cdot\mathbf{E}(t), \tag{4}$$

where $V_{n,1}$ and $V_{n,2}$ are the nuclear binding potentials experienced by the two electrons, $V_{ee}(r_{12})$ is the electron-electron repulsion, and $e = -|e|$ is the electron's charge. Guidelines have never been found that allow these five interactions to be ordered on the basis of increasing strength or importance, so ideally they must be treated on an equal basis. However, approximations have been based on the rationale that different subsets can be identified as dominant at different stages of the double-ionization process.

Therefore, methods fall into two camps, which we call the "step-by-step" camp and the "all-at-once" camp. The step-by-step approach uses stepwise calculations, usually based on a sequence of stages supposed to be taking place in the NSDI process, in this way obtaining predictions for specific observations. Different atoms or different experimental conditions may force one to consider different stages. Also, different authors may highlight different physical stages as key and take slightly different calculational steps. The all-at-once approach takes the set of fundamental interactions of the electrons and approximately solves their basic equations of motion without predetermined ideas about an underlying sequence of stages. The resulting global solutions are then used for comparison with specific experimental data.

An all-at-once attack on a complicated problem has only become feasible due to today's computing facilities. Historically, necessity always enforced some sort of step-by-step approach. However, it is interesting to note that conceptual clarity derives more easily from a step-by-step approach, even though this might come at the expense of closeness to physical reality. For example, the all-at-once approach does not impose the clean-cut separation between sequential and nonsequential mechanisms that accompanies the step-by-step approach. Experimental data are, of course, always obtained in an all-at-once fashion.

B. Step by step: Tunneling and recollision

In 1964, working with the basic concepts mentioned in Sec. I, Keldysh (1964) made an inspired nonperturbative innovation by proposing an *ad hoc* scenario for high-field one-electron ionization. This was the first use of the step-by-step approach. He combined the fact that a strong laser field lowers the binding potential into a finite barrier with the fact that a laser's oscillations are essentially static on the time scale of the Bohr-frequency oscillations of an electron in a bound orbit. This boldly exported the traditional static view of tunneling ionization into the optical domain.

Thirty years later Corkum (1993) proposed adopting the same view for double ionization. He noted that an electron, after tunneling, could in the next half cycle be returned by the laser field to the ion core, where it could have acquired enough energy from the field to knock out a second electron. Qualitatively, this had already been proposed by Kuchiev (1987). Double ionization of this form would not be a simple succession of independent ionization events. Instead, after tunneling free the first electron is considered to initiate double ionization by a laser-driven collision (in the literature usually called a recollision or a rescattering). The recollision scenario, sketched in Fig. 2, is obviously highly correlating and fits the NSDI label perfectly.

Further theoretical development, and acceptance, of the step-by-step approach based on the tunneling-recollision scenario came gradually. The early stage focused on the one-electron transition amplitude that Keldysh wrote, as if the ionization transition were caused by a first-order dipole interaction of the electron with the laser field $\mathbf{E}(t)$. It took the form

$$M_{\mathbf{p}0} = -i \int_{-\infty}^{\infty} dt \langle \psi_{\mathbf{p}}^{\mathrm{V}}(t) | [-e\mathbf{r} \cdot \mathbf{E}(t)] | \psi_0(t) \rangle, \tag{5}$$

where the usual dipole-interaction Hamiltonian has been taken in the length gauge, $H_I(t) = -e\mathbf{r} \cdot \mathbf{E}(t)$, and $|\psi_0(t)\rangle$ is the electron's initial (bound) state. Keldysh's second innovation was, in the final continuum state, to replace the customary plane wave by a Volkov state $|\psi_{\mathbf{p}}^{\mathrm{V}}(t)\rangle$ (Wolkow, 1935):

$$\psi_{\mathbf{p}}^{\mathrm{V}}(\mathbf{r}, t) = (2\pi\hbar)^{-3/2} \exp\left\{\frac{i}{\hbar}[\mathbf{p} - e\mathbf{A}(t)] \cdot \mathbf{r}\right\} \times \exp\left(-\frac{i}{2m\hbar} \int^{t} d\tau [\mathbf{p} - e\mathbf{A}(\tau)]^2\right), \tag{6}$$

where $\mathbf{p}$ is the average (drift) momentum of the electron in the laser field $\mathbf{E} = -d\mathbf{A}/dt$. The importance of the second innovation by Keldysh is the nonperturbative "all-orders" character obtained from the exponentiated vector potential in Eq. (6). Volkov states were first utilized by Reiss (1962) in external-field problems in quantum electrodynamics, such as laser-induced electron-positron pair creation.

From the square of the matrix element (5), a total transition rate was calculated by integrating over the final momenta $\mathbf{p}$. In the limit where the ponderomotive energy exceeds

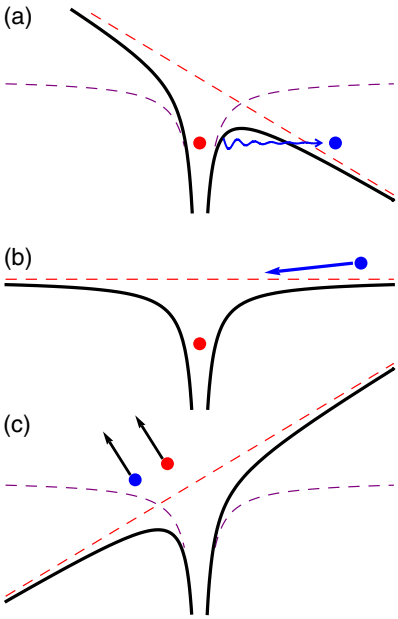

FIG. 2 (color online). An artist's sketch of a recollision process leading from tunneling emission of one electron (a), through its laser guidance back onto the ion (b), to recollision and double ejection (c).

the ionization potential, i.e., where the so-called Keldysh parameter

$$\gamma \equiv \sqrt{\frac{I_P}{2U_p}} \tag{7}$$

is small compared with unity ($\gamma \ll 1$), the transition rate can be approximated by a form familiar from static tunneling theory (Landau and Lifishitz, 1977),

$$w(t_0) \sim \frac{1}{|E(t_0)|} \exp\left\{-\frac{2}{3}\frac{(2I_P)^{3/2}}{|E(t_0)|}\right\}. \tag{8}$$

Here $E(t_0)$ is the value of the laser field at the moment of tunneling (Yudin and Ivanov, 2001b). In the rate (8), the exponential is a very general feature, while prefactors can depend on Coulomb or other corrections.

The Keldysh scenario, reformulated by Perelomov *et al.* (1966), applied by Faisal (1973), and extensively developed by Reiss (1980), has been very widely used and further extended to the two-electron theme. Along with small variations this approach is often indicated by the initials KFR of Keldysh, Faisal, and Reiss and has become also known as the strong-field approximation, often abbreviated SFA. Reiss (2008) showed that the SFA suggests some restrictions on applicability of tunneling theory to photoionization. Depending on wavelength and intensity, these restrictions identify a "safe" zone where the concept of static tunneling can be applied for a nonstatic field. Most near-optical wavelength experiments fall within it. One should add that despite its successes it is very hard to say exactly in which sense the SFA is an approximation. For example, a systematically ordered sequence of successive higher order corrections has never been agreed on. Nevertheless, we describe below the way it has been extended to include the second electron's ejection by various collision interactions, following the Corkum proposal. This later extension to double ionization describes what is often called a three-step process.

We note that the Keldysh ansatz fits with the step-by-step approach in a rather straightforward fashion. It neglects the electron-field interaction $-e\mathbf{r}\cdot\mathbf{E}(t)$ before ionization, and the binding potential $V(r)$ after ionization. In this sense, the integral over time t in the matrix element (5) is an integral over an ionization time. The SFA as formulated in Eq. (5) can readily be extended to include a recollision (Becker *et al.*, 1994; Lewenstein *et al.*, 1995), and this has become the basis for the development of a two-electron SFA formalism (see Sec. IV.C).

C. Step by step: "Simpleman" kinematics

Obviously, the recollision picture imposes a specific view of NSDI as a process that develops as a train of separate events: At some time t_0 in the laser field, one electron is considered to tunnel to freedom, emerging on the slope of the down-turned Coulomb potential with zero velocity in the direction of the laser polarization as shown in Fig. 2(a). The second electron is temporarily entirely ignored, implicitly invoking the SAE approximation, as is the effect of the Coulomb field of the ion on the tunneled electron, whose motion under the laser influence alone is supposed to follow a completely classical trajectory with velocity $\mathbf{v}(t)$. This view has been known as the simpleman picture of one-electron ionization since early studies of above-threshold ionization (van Linden van den Heuvell and Muller, 1988) and this picture remains quite useful.

Depending on the field phase at the ionization time t_0, the electron's simpleman velocity along its laser-driven classical trajectory is

$$\begin{aligned} m\mathbf{v}(t) &= m\mathbf{v}(t_0) + e\int_{t_0}^{t}\mathbf{E}(t')dt' \\ &= m\mathbf{v}(t_0) + e[\mathbf{A}(t_0) - \mathbf{A}(t)]. \end{aligned} \tag{9}$$

Assuming that at $t = t_0$, at the end of the tunnel, the electron emerges with zero velocity [$\mathbf{v}(t_0) = 0$] and that the vector potential outside the laser pulse vanishes, we infer that at the detector the electron's momentum (its drift momentum) is $e\mathbf{A}(t_0)$, reflecting its time of birth t_0. Now, at a later time $t_{\rm rec} > t_0$ the electron may return to the position of the ion with sufficient energy to induce ejection of the second electron, producing a double-ionization "recollision" as illustrated in Figs. 2(b) and 2(c). A quick calculation based on Eq. (9) then shows that the returning kinetic energy $E_{\rm ret}$ has the maximum value (Corkum, 1993; Kulander, Schafer, and Krause, 1993; Schafer *et al.*, 1993)

$$E_{\rm ret}|_{\rm max} = 3.17\ U_P, \tag{10}$$

and this occurs for electrons that are set free shortly after the electric-field peak ($\frac{1}{20}$ of the period). The corresponding time $t_{\rm rec}$ of recollision is very close to the second-to-next zero crossing of the field.

Provided the kinetic energy of the recolliding electron exceeds the second ionization potential I_{P2}, the second electron (assumed quiescent in the meantime) may be released into the continuum. Having shared the overshoot of the return energy $E_{\rm ret}$ over the second ionization potential I_{P2}, both electrons are then again treated as free of Coulomb forces, responding to the laser field alone, and acquiring additional drift momenta $e\mathbf{A}(t_{\rm rec})$ [cf. Eq. (9)] that carry them to the detector. From this simpleman "recollision–impact-ionization" (RII) scenario, we then expect that the electrons are ejected side by side with their momenta distributed about the common drift momentum in the direction of the (linearly polarized) field

$$|p| = |eA(t_{\rm rec})| \approx \max|eA(t)| = 2\sqrt{mU_P}. \tag{11}$$

The width of the distribution is given by the aforementioned overshoot energy.

By momentum conservation, the ion will have a momentum opposite to the total momentum of all electrons. So it will be distributed around the value $P_\parallel = 4\sqrt{mU_P}$ for NSDI and around $2N\sqrt{mU_P}$ for N-fold nonsequential ionization. This simple prediction can be compared with Fig. 3, which shows the measured yield of doubly and triply ionized neon plotted versus the final ion momentum. The nominal intensities yield $P_\parallel = 6.7$ a.u. ($N = 2$) and $P_\parallel = 10.8$ a.u. ($N = 3$), which are above the measured values of $P_\parallel \sim 4$ and ~ 7 a.u., respectively. Still, given the uncertainty of the experimental intensities, the distribution of the yield is well compatible

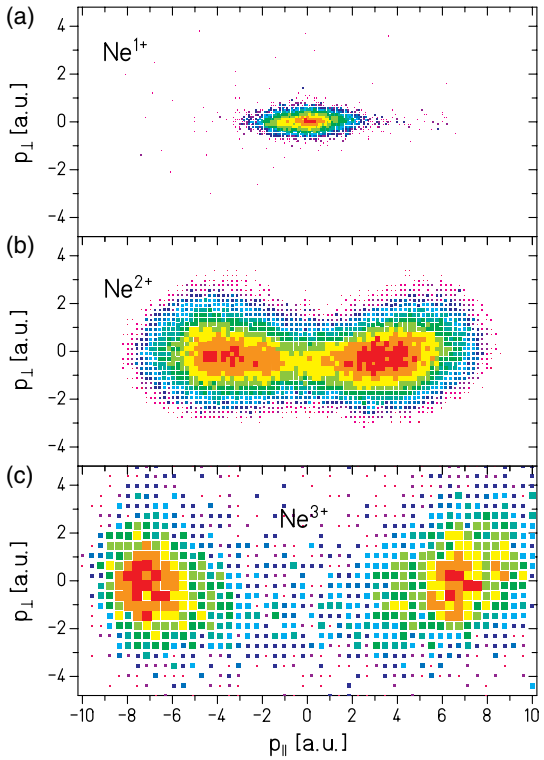

FIG. 3 (color online). Two-dimensional momentum distributions $(P_{\parallel}, P_{\perp})$ of Ne^{N+} ions ($N = 1, 2, 3$) at peak intensities of 1.3 PW/cm^2 ($N = 1, 2$) and 1.5 PW/cm^2 ($N = 3$) and a wavelength of 795 nm [(a)–(c), respectively]. The distributions are integrated over the third Cartesian ion-momentum coordinate. Note how the distribution dramatically widens in the transition from single to multiple ionization. From Moshammer *et al.*, 2000.

with the simple picture presented above. We return to the discussion of these data in Sec. V.D.

Looking ahead, we find that the simpleman picture provides steady points of reference in the remainder of our discussion. We see that classical simulations can support the recollision element fully while discarding tunneling completely. We remark, however, that the model, based on the one-electron tunneling postulate dating from Keldysh, has become so ingrained that one tends to ignore that it is still basically a speculative conjecture and strongly reliant on the validity of the SAE approximation. Two simultaneously active and interacting electrons could, in principle, tunnel out at the same time, and "collective tunneling" by two electrons was considered (Zon, 1999; Eichmann *et al.*, 2000). Currently available data provide no basis for its occurrence in NSDI. However, collective tunneling is predicted to contribute to tenfold and higher ionization of rubidium (Kornev, Tulenko, and Zon, 2009).

The relevance of the recollision process is not restricted to NSDI. Since attosecond pulses are generated in a recollision, it is at the core of the emerging field of attosecond physics. Recollision is also becoming an important framework for conceptual understanding of new forms of electron scattering with unprecedented spatial and temporal precision; see Niikura and Corkum (2006), Krausz and Ivanov (2009), and Corkum (2011).

D. All-at-once double-ionization theory

A complete theoretical description of an ionization event, free of any ansatz and intuitive picture, is obtained by an exact solution of the time-dependent Schrödinger equation (TDSE):

$$i\hbar\frac{\partial}{\partial t}\Psi(\mathbf{r_1},\mathbf{r_2},t) = \Big(-\frac{\hbar^2}{2m}\Delta_1 - \frac{\hbar^2}{2m}\Delta_2 + V_{n,1}(\mathbf{r}_1) + V_{n,2}(\mathbf{r}_2) + V_{ee}(r_{12}) - e(\mathbf{r}_1+\mathbf{r}_2)\cdot\mathbf{E}(t)\Big)\Psi(\mathbf{r_1},\mathbf{r_2},t). \quad (12)$$

The solution to Eq. (12) represents the ideal conclusion to an all-at-once kind of theoretical approach as well as the optimum target for experimental comparison. An analytic solution is beyond reach but the steady development of computer technology has made limited numerical work feasible. Time-dependent Hartree-Fock and density-functional methods are not very satisfactory for high-order ionization in strong fields, which requires highly accurate representation of states far from the ground state. For single ionization, the development of grid-based integration schemes with careful implementation of the SAE approximation made *ab initio* numerical solutions of the TDSE feasible beginning about 1985 (Kulander, 1987); for a review, see Kulander, Schafer, and Krause (1991).

Two-electron TDSE numerical wave functions present a challenge even now, because of computer speed and memory requirements. For NSDI there is only a narrow range of results, obtained from calculations with a low number of active dimensions or restricted to wavelengths shorter than those commonly used experimentally. A second numerical all-at-once approach to high-field two-electron physics is based on the use of the time-dependent Newton equations (TDNE) to obtain classical NSDI electron trajectories. Such calculations are motivated by striking similarities (see Fig. 4) between classical TDNE and quantum TDSE probability distributions. This qualitative agreement, together with the ease of solving ordinary versus partial differential equations, motivated extensive TDNE explorations of NSDI leading, even though completely classical, to a number of predictions

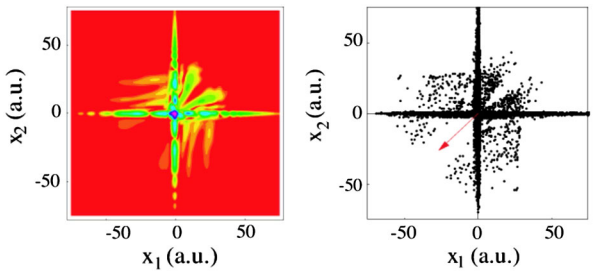

FIG. 4 (color online). Quantum TDSE (left) and classical TDNE (right) spatial distributions of positions of electrons undergoing NSDI midway through a laser pulse. The aligned-electron approximation (AEA; see Sec. IV.A) and the same model potentials, laser wavelength, pulse shape, and intensity were employed for both calculations. Particularly notable is the common emergence of NSDI "jets" of electron pairs into the upper right quadrants. From Panfili, Eberly, and Haan, 2001.

with at least semiquantitative agreement with a relatively wide variety of experimental data.

III. BASIC EXPERIMENTAL FACTS

Experiments have exposed several different aspects of NSDI electron behavior. Initial ion-count results provided the first evidence that unusual $e-e$ correlation effects are involved. Characteristic double-ionization data were shown in Fig. 1. NSDI events are clearly orders of magnitude stronger than sequential tunneling theory predicts at intensities below the onset of the conspicuous knee in the curve. This shape of the doubly charged ion curve has been found in all species of atoms tested to date. Early clues to the physics of NSDI were provided by the fact that no knee was observed at a laser wavelength of 248 nm (Kondo *et al.*, 1993) and that the knee quickly disappeared with increasing ellipticity of the driving laser field (Fittinghoff *et al.*, 1992; Dietrich *et al.*, 1994).

Later experiments using the cold-target recoil-ion-momentum spectroscopy (COLTRIMS) technique (Dörner *et al.*, 2000) or, more generally, the so-called reaction microscope, added end-of-pulse momentum distribution data. A cold atomic-gas target is a prerequisite for the recoil-ion-momentum measurements, since the thermal momentum spread (i.e., the initial momentum spread) of the target must be smaller than the recoil-ion momenta during the interaction of the atoms with the strong laser field. As coincidence experiments, they faced and overcame several challenges. For example, no more than one ionization event should be allowed to occur per laser shot, in order that all the resulting electrons can be traced to the same event. This mandates low target density. It means that each laser shot provides a (at most) one-atom experiment, and so puts a high premium on the laser repetition rate and stability of wavelength and intensity over the course of a run. Current Ti:sapphire lasers reached repetition rates of about 6 MHz at sufficient energy per pulse (Liu *et al.*, 2008).

If we neglect the momentum of the laser photons, which is an excellent approximation in the present context, then owing to momentum conservation double ionization is fully characterized by six momentum components, the momenta either of the two electrons or of one electron and the ion. In most COLTRIMS experiments, not all of the momentum components are actually observed. This means that the remaining components are in fact summed over (or, sometimes, restricted to some finite intervals). The very first NSDI COLTRIMS experiments (Moshammer *et al.*, 2000; Weber *et al.*, 2000b) focused on the ion momentum and presented just its longitudinal component (the one parallel to the axis of the laser polarization) or, in addition, one transverse component, with all remaining components summed over. We showed an example in Fig. 3.

An important role was played by the analysis of the electron-electron momentum correlation, the first example of which (Weber *et al.*, 2000a) is reproduced in Fig. 5. The figure shows the yield of NSDI versus the end-of-pulse longitudinal momentum components of the two electrons, again with the other components completely integrated over or confined to certain ranges. Since the ion momentum is the opposite of the sum of the two-electron momenta, the ion-momentum distribution in the fashion of Fig. 3 can be obtained by projecting the momentum-momentum distribution on the $k_{x1} = k_{x2}$ diagonal. Since the two electrons cannot be distinguished, the distributions should be symmetrical with respect to the main diagonal and, provided the laser pulse is sufficiently long, also with respect to the off-diagonal ($p_1 \leftrightarrow p_2$ and $p_1 \rightarrow -p_1$, $p_2 \rightarrow -p_2$, respectively). These expected symmetries allow experiments to be concentrated in a restricted range of momenta, and plots such as in Fig. 5 exploit these symmetries to fold limited data into all four quadrants, as its perfect symmetries make evident.

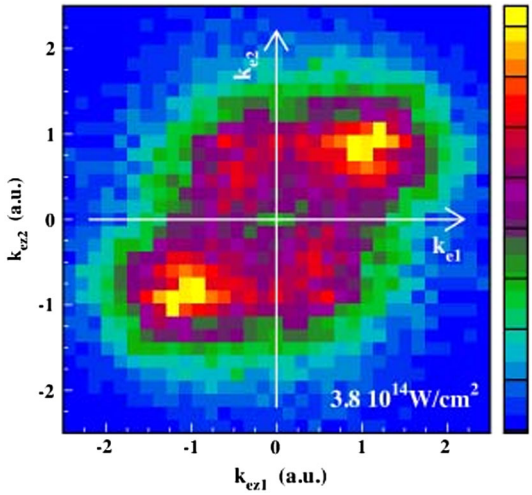

FIG. 5 (color online). Momentum-momentum correlation of the two electrons emitted in NSDI of argon below saturation by a Ti:sapphire laser with a peak intensity of 3.8×10^{14} W/cm^2. From Weber *et al.*, 2000a.

Almost any NSDI report has presented the data in the form of one of these three plots: the ion yield as a function of intensity as in Fig. 1, the ion yield for fixed intensity as a function of the ion's momentum components as in Fig. 3, and the ion yield for fixed intensity as a function of the longitudinal momenta of the two electrons as in Fig. 5. The total ion yield as a function of intensity tells immediately whether ionization proceeds sequentially or not: The sequential process, when interpreted as two independent tunneling events, can be calculated in a straightforward fashion (represented by the solid line in Fig. 1). Any significant deviation from this scenario then points to the presence of a nonsequential pathway.

In contrast, the ion yield as a function of the ion momentum does not have an unambiguous signature of nonsequentiality. However, it affords important clues for the mechanism of a nonsequential process. For example, the double-humped ion-momentum distribution, a representative of which is exhibited in Fig. 3(b), strongly points to recollision as the responsible mechanism. Recall that if both electron momenta have distributions centered about the value (11), then the ion momentum will be centered about the values $P_{x\text{ion}} = \pm 2p_x = \pm 4\sqrt{mU_P}$. Indeed, this can be observed in Fig. 3(b).

The e-e momentum correlation, as shown in Fig. 5, gives the most detailed information about the mechanism of the

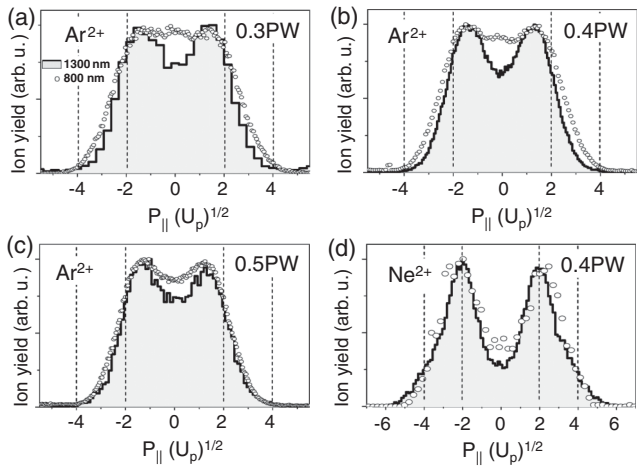

FIG. 6. Longitudinal ion-momentum distribution for double ionization of (a)–(c) Ar and (d) Ne at 1300 nm (solid lines) and 800 nm (open circles). Intensities in PW/cm^2 are given in the panels. From Herrwerth *et al.*, 2008.

nonsequential process. Figure 5 clearly shows the footprint of a recollision pathway in the strong population maxima centered about $p_{x1} = p_{x2} \approx \pm 2\sqrt{mU_P}$. However, there is also significant population in the second and fourth quadrants representing electrons that are emitted back to back, which is incompatible with the recollision–impact-ionization scenario. Up to fourfold differential cross sections have been measured by now with the help of the reaction microscope (Weckenbrock *et al.*, 2004), but most of the interpretation has been based on the 2D *e*-*e* correlation.

The data observed vary from atom to atom, but in a rather narrow sense, as shown in Fig. 6. For example, the ion-momentum distributions may or may not display a dip or a reduced population density, respectively, around zero momentum. This depends on the atomic species, but also on the laser intensity and frequency (Alnaser *et al.*, 2008; Herrwerth *et al.*, 2008), and plays an important role in the interpretation of the data.

IV. DESCRIPTION OF THEORETICAL MODELS

This is the central section of our overview. Here we present the principal theoretical approaches to high-field double ionization. There are two that use the all-at-once approach: (A) the direct quantum-numerical approach, i.e., the solution of the two-electron TDSE numerically, and (B) its completely classical analog TDNE, i.e., the use of large collections of numerical solutions of the corresponding classical Newtonian equations. In contrast, two others use the step-by-step approach: (C) a quantum recollision theory in a Feynman diagram (FD) setting, a two-electron modification of the Keldysh-SFA ansatz that makes quantum-mechanical calculations in the three-step recollision sequence of events, and (D) a flexible tunneling-classical (TC) blend of approaches that takes quantum tunneling as the initiator of ionization and then uses Newtonian theory to make classical calculations in the step-by-step recollision sequence. These four will be described in the following. In Sec. V we compare the results of the various approaches with selected experimental data for illustration.

All four approaches (with the single exception of the TDSE treatment of atomic helium) need to incorporate an approximate or modeled treatment of the ion core. This typically involves some kind of shielding of the ion's Coulomb potential and may also include *ad hoc* modifications of the *e*-*e* potential, which is then considered an effective potential. These modifications can and typically do depend on the species, and in the FD approach can also depend on the specific recollision sequence being calculated.

A. Quantum-numerical solutions for helium and other atoms

In high-field atomic theory a solution of Eq. (12), the TDSE, can be taken as the ultimate goal. Numerically exact two-electron solutions of the TDSE require well-developed computational methods and resources. A number of approximations and shortcuts characterized the first TDSE attacks on NSDI. The simplest case (recall Fig. 4), using only one dimension, is partially justified by the so-called "aligned-electron approximation" (AEA) [see Javanainen, Eberly, and Su (1988)], which is prompted by the assumption that in NSDI experiments the electrons are mainly driven linearly, along the polarization axis of the field, given the almost exclusive experimental use of linear polarization. An artificial transverse degree of freedom was introduced by using for the Coulombic *e*-*e* repulsion a "soft-core" potential [see Eq. (16)] and this allows two electrons to pass each other in one dimension. The early attempts by Grobe and Eberly (1992) to solve for numerical wave functions for two-electron ejection were restricted in this way. A number of groups pursued variants of this approach (Bauer, 1997; Liu *et al.*, 1999; Haan *et al.*, 2000, 2002; Popov, Tikhonova, and Volkova, 2001; Prauzner-Bechcicki *et al.*, 2007). The results showed features recognizably similar to experimental findings, but without consistent quantitative agreement as to absolute ionization yields or intensity dependences.

Taylor's Belfast group has made a long-running and successful attack on NSDI theory of helium via the TDSE approach in all three space dimensions (Parker *et al.*, 2001, 2003, 2006, 2007). This is the one TDSE calculation for which no questions can arise about core electron effects, since there is no core. The demands on computational technique are extreme. The reasons for this are easily seen when one takes into account the need for spatial resolution on the atomic scale, well below 1 Å inside the atom while outside a larger grid may be adopted, along with the need to allow for a spatial grid as large as the excursion amplitude α_L of an electron oscillating under control of the laser field. This amplitude, as a multiple of the Bohr radius, is given by

$$\alpha_L = |e|E_0/m\omega^2 = (|e|E_0/m)(\lambda/2\pi c)^2 = 2.6 \times 10^{-12}\sqrt{I}\lambda^2, \quad (13)$$

when I is given in W/cm^2 and λ is in nm.

At an intensity of 4×10^{14} W/cm^2 (which is a typical value, although intensities 10 times higher have been used for helium) and for $\lambda = 800$ nm we have $\alpha_L = 330$ Å. (Recall that this oscillation is transverse to the propagation direction

of the laser field, so even an order of magnitude greater excursion, requiring 2 extra orders in intensity, would not seriously compromise the dipole approximation.) For two electrons this then implies a computational field that may need to hold 10^3 grid points in active memory for each dimension, or possibly 10^{15}–10^{16} points in total, and to change rapidly enough to resolve fractions of an optical cycle accurately. Since α_L is proportional to the square of the laser wavelength, these requirements are reduced for shorter wavelength light, but there are little data for comparison.

Despite the obvious difficulties, the Belfast group has made significant progress. Their HELIUM code (Smyth, Parker, and Taylor, 1998; Moore *et al.*, 2008) is designed to run with high efficiency on distributed-memory massively parallel computers. It is capable of dealing with arbitrary polarization, although linear polarization, which reduces the degrees of freedom by 1, is normally used. In all cases, the two radial variables r_1 and r_2 are modeled on a finite-difference grid, while the angular variables θ_1, θ_2, ϕ_1, and ϕ_2 are handled by a basis set of coupled spherical harmonics (partial waves).

One must add, however, that important information coming from both the helium fundamental TDSE work and the fully dimensioned classical simulations to be mentioned below, encourages continued TDSE attacks of intermediate rigor. For example, one knows that the laser-atom interaction energy $-\mathbf{d}\cdot\mathbf{E} = -e(\mathbf{r}_1+\mathbf{r}_2)\cdot\mathbf{E}$ couples the field only to the electron pair's center of mass. This suggests that little harm will be done by allowing the AEA to be applied to their center-of-mass coordinate, while permitting the relative coordinate $\mathbf{r}_1$–$\mathbf{r}_2$ to evolve full dimensionally under the local Coulomb forces. Such an approach was pioneered by Ruiz *et al.* (2006) and successfully applied in situations where the full solution is not feasible.

We note for all-at-once theories that quantum TDSE solutions will automatically preserve all proper symmetries of the initial conditions. In contrast, distributions made from collections of classical TDNE solutions will not, because a random initial microcanonical TDNE distribution of a finite number of electron pairs can only approximately obey an exact symmetry condition. Thus the quantum TDSE wave function in Fig. 4 was started with a properly symmetric initial state and remains perfectly symmetric at the later time of the snapshot, whereas the TDNE distribution in the figure shows very slight asymmetries, reflecting the imperfect symmetry obtained from a random microcanonical initial assignment of momenta and positions among only 25 000 electron pairs.

Obviously, even when a numerical solution of the TDSE is accomplished, this usually does not easily afford the kind of understanding that is based on analytical formulas. However, numerical time-dependent wave functions do afford interpretive capabilities not shared by other numerical methods. For example, one can perform a quantum analog of the classical "back analysis" described in Sec. IV.B. That is, the part of a TDSE wave function showing two-electron release (i.e., the portion where both electrons have traveled far from the nucleus at the end of the pulse) can, in principle, be numerically selected by masking out the remainder and then propagated separately backward toward $t = 0$. Such backpropagation allows close insight into the history of a successful NSDI event, almost the same as having true quantum trajectories of two-electron motion leading to NSDI. Such backpropagated trajectories have already been calculated in limited cases. This was under dimensional restrictions (Haan *et al.*, 2002; Panfili, Haan, and Eberly, 2002), while still providing additional insight into the character of NSDI events, particularly about the formation of correlated two-electron "jets" of probability en route to double ionization.

Another example is provided by the intriguing question whether NSDI is an intrinsically quantum process or perhaps partly or even mostly classical in character. An intrinsically quantum character can be associated with the extent to which the two-electron function is nonseparable, i.e., entangled, and the question is open to answer by the Schmidt analysis; see Grobe, Rzążewski, and Eberly (1994) and Liu *et al.* (1999). Numerical reorganization of an NSDI wave function can recast it in Schmidt format. Such a wave function is a sum of canonical eigenpairs, products of orthogonal single-particle states. The effective number of the pairs signifies the quantum entanglement of the two electrons and thus gives a quantitative measure of the true "quantumness" of the NSDI state. One such test made under a dimensional restriction (Liu *et al.*, 1999) suggests that NSDI may have a surprisingly small quantum character.

Another opportunity afforded by any TDSE approach is the ability, in principle, to perform a quantum analog of classical back analysis described in Sec. IV.B. The usually small portions of any outgoing numerical TDSE wave function that represent double ionization can, in principle, be numerically masked and propagated backward in time. Such backpropagation allows unusual insight into the origin of a successful NSDI event, almost the same as having true quantum trajectories of two-electron motion leading to NSDI. These backpropagated trajectories can also be compared to fully classical trajectories, providing additional insight into the quantum character of NSDI events. Such comparisons have been made, but so far with dimensional restrictions (Haan *et al.*, 2002; Panfili, Haan, and Eberly, 2002).

Short of the *ab initio* numerical solution of the two-electron TDSE without any simplifying assumptions, there have been numerous other attempts, with the intention to make the problem more feasible and/or to allow one to treat atoms other than helium. We are content with mentioning time-dependent density-functional methods (Bauer and Ceccherini, 2001; de Wijn, Lein, and Kuemmel, 2008), and methods that are built on using certain basis sets for the coupled quantum equations, such as the coupled-coherent-states method (Shalashinin, Child, and Kirrander, 2008; Guo, Liu, and Chu, 2010), the time-dependent multiconfiguration Hartree method (Sukiasyan *et al.*, 2009), and the time-dependent configuration-interaction singles method (Greenman *et al.*, 2010). Recently the numerical methods (finite-difference representation, Arnoldi time propagator) of the HELIUM code mentioned above have been combined with *R*-matrix techniques to construct the RMT code (*R*-matrix incorporating time) (Nikolopoulos, Parker, and Taylor, 2008; Moore *et al.*, 2011). RMT makes possible accurate

calculations of a multielectron response leading to single ionization in complex multielectron atoms in intense-laser fields. However, thus far none of these approaches has produced results that allow for a direct comparison with experimental NSDI data.

B. Completely classical trajectories

The approach that is conceptually closest to the TDSE approach is the TDNE approach, in which one numerically solves Newton's equations for the electrons rather than Schrödinger's equation. The ease of solving ordinary, as opposed to partial, differential equations makes the TDNE approach much easier to implement in practice, and TDNE calculations can be carried out over the wide range of wavelengths, pulse lengths, and laser intensities where most experiments have been done. As with the TDSE approach, it has no need at any stage for perturbation theory. It shares the central advantage with TDSE that it is also based on a fully holistic or all-at-once view of the complicated multiple interactions that the electrons undergo.

TDNE analysis has a long history, and in the high-field domain of atomic physics dates at least to a calculation of He and Be double ionization, in advance of the wide recognition of definitive ion-count knees, by Wasson and Koonin (1989). Strong motivation for further work was provided by the striking similarity found by Panfili, Eberly, and Haan (2001) between TDNE and TDSE probability distributions made under identical AEA conditions, already shown in Fig. 4. In the most recent decade the wide variety of classical ensemble calculations made for atomic and molecular double ionization can be divided into two categories: those allowing a random microcanonical position-momentum ensemble to determine initial conditions, and those imposing a quantum-style tunneling startup in the middle of the laser pulse. We focus here on the former and explain the latter in Sec. IV.D.

The Newtonian equations to be solved, written in atomic units ($\hbar = m = |e| = 4\pi\epsilon_0 = 1$), which we use consistently from now on, are completely ordinary:

$$\frac{d^2\mathbf{r}_i}{dt^2} = -\mathbf{E}(t) - \boldsymbol{\nabla}_{\mathbf{r}_i}(V_{n,i} + V_{ee}), \tag{14}$$

for $i = 1, 2$, which follow from the Hamiltonian (4) with the potentials defined in a way to model the effect of core electrons, as described below. The initial conditions on position and velocity are selected randomly from an ensemble, which can be determined in one of several practically equivalent microcanonical ways, such that the total energy, kinetic plus potential, is the atom's actual two-electron ground-state energy.

In usual TDNE practice one takes a linearly polarized laser field:

$$\mathbf{E}(t) = E_0 f(t)\hat{\mathbf{x}}\sin(\omega t + \phi), \tag{15}$$

where $f(t)$ is an envelope slow enough to be treated adiabatically, and whose time dependence can frequently be ignored completely. An example can be found in the uppermost row of Fig. 7. In each numerical experiment, the phase ϕ of the laser field is given a random value at $t = 0$ when the field envelope function $f(t)$ smoothly turns on. Smooth turnons have been modeled mostly by pulses with trapezoidal or sine-square envelopes.

From one point of view, the TDNE approach is a way to make experiments in the same way as in the laboratory, i.e., one atom (two electrons) at a time, in a very long sequence of laser shots. The outcomes of these numerical experiments can be collected into distributions displaying counts of singly, doubly, and multiply ionized ions, as well as electron and ion momenta and energies, just as is done with data of the same type recovered in the laboratory. Laboratory outcomes obviously depend on laser intensity, wavelength, and pulse duration as well as polarization, and on atomic species. All of these are available for adjustment from one numerical TDNE experiment to the next, just as in laboratory work.

An important feature of both TDSE and TDNE simulations is that they are independent of the recollision conjecture and obtain results on the basis of dynamical equations alone. Nevertheless, they support that conjecture in a number of ways. Two examples are given in Fig. 7. From the TDNE electron trajectories depicted, the existence of a recollision time is eye catching and its value precisely defined. The trajectories also show that one electron is ionized at some time while the other one remains bound, even though the precise value of the ionization time depends on its definition. The existence of a small delay between rescattering and the final departure time, when both electrons leave the vicinity of their parent ion, is also suggested. These TDNE results support the three-step model and lend credibility to the FD method, and the statistical model derived from it

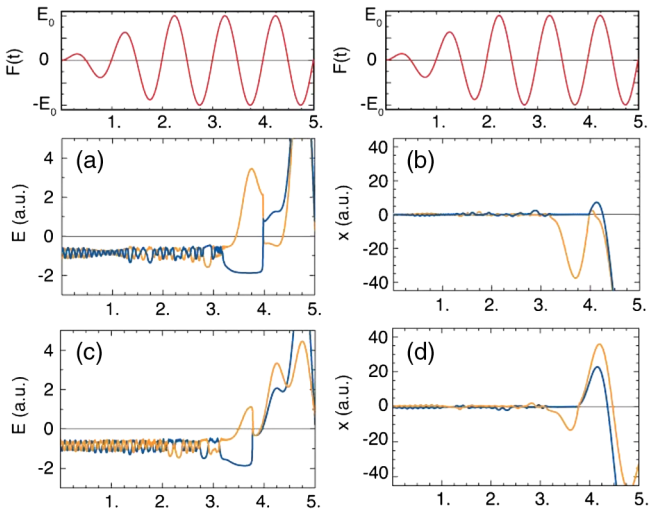

FIG. 7 (color online). Time evolution of the total energy of each NSDI electron during the first five laser cycles. The top panel of each column plots the time evolution of the laser electric field $E(t)$ with the peak amplitude E_0. The remaining panels of each column display the energy E and the transverse displacement x of the two NSDI electrons of a trajectory. The second and third rows depict typical NSDI events with comparatively long ($t_{\mathrm{rec}} - t_0 > 0.5T$) and short ($t_{\mathrm{rec}} - t_0 < 0.5T$) "travel" time intervals, respectively. The horizontal axes are labeled by multiples of the laser period T. The plots are obtained with the soft-core Coulombic e-e repulsion potential (16). The light and dark curves refer to the recolliding and the bound electron, respectively. From Ho, 2007.

(see Sec. VI.G), as well as the TC method's assumption of a definite ionization time.

The obvious TDNE disadvantage is the abandonment of quantum mechanics, which is certainly the correct underlying theory of atomic phenomena. However, the ability of the TDNE method to deal with experimental results is surprisingly strong, and what really matters is whether contradictions of principle play a role in practice. Given the comparison in Fig. 4, it is perhaps not surprising that the TDNE approach has achieved a substantial degree of validity, to accompany its ease of implementation. TDNE results provide unique opportunities to decide if specific features of NSDI are in fact quantum mechanical in character, or possibly not (Ho and Eberly, 2005). Of course, the most fundamental quantum-classical distinction is the possibility of particle-wave interferences in quantum theory, but so far these have played no role in NSDI experiments.

TDNE theory has several options regarding energy levels and ionization potentials, which must be treated phenomenologically. The binding energy is easily established as the negative sum of the first and second ionization potentials, typically taken from tables. For example, for Kr these are 13.999 and 24.359 eV, which together yield a binding energy of 38.358 eV = 1.41 a.u. The Hamiltonian is the same as the fundamental form in Eq. (4), but the nuclear and $e-e$ potentials may be expressed functionally in a variety of ways: e.g., Coulombic with a soft core (Javanainen, Eberly, and Su, 1988; Su and Eberly, 1991), short-range Yukawa (Ho, 2007; Ho and Eberly, 2007), or Fermi molecular dynamics (Wasson and Koonin, 1989; Lerner, LaGattuta, and Cohen, 1994; LaGattuta and Cohen, 1998). Most of the recent TDNE work has adopted the soft-core form, where $V_{n,i}(r_i)$ and $V_{ee}(r_{12})$ are replaced with soft-core truncations at shortest range (Javanainen, Eberly, and Su, 1988; Su and Eberly, 1991):

$$V_{n,i}(r_i) = -\frac{2}{\sqrt{r_i^2 + a^2}}, \quad V_{ee}(r_{12}) = \frac{1}{\sqrt{r_{12}^2 + b^2}}, \tag{16}$$

identical for each electron.

The numerical value of a is chosen to prevent autoionization, and a typical value is in the range 0.8–2.0, whereas normally $b \approx 0.1$ or smaller. The quantity $r_{12} = |\mathbf{r}_1 - \mathbf{r}_2|$ denotes the distance between the two electrons. The Hamiltonian with the soft-core potentials defines the TDNE model atom. Manipulation of the two shielding parameters a and b can be regarded as the TDNE approach to core theory for different atomic species. The value of b has a significant effect on the electron trajectories and the electron spectra. Haan and Smith (2007) and Haan, Van Dyke, and Smith (2008) examined a hybrid TDNE model in which the a parameter was manipulated dynamically. One could also investigate the effect of the magnitude of the shielding parameter b or entirely different potential forms, such as a Yukawa potential, which allows one to consider the transition to a short-range potential (Ho, 2007).

Because of the simplified model potentials used, in its most common application the TDNE approach is intended as a generic rather than specific theory. This is the reason that in a number of applications the zero-field energy of each 2-e member of the ensemble is initially set to be −1.3 a.u. as a way to approximately model the binding energies of both xenon (−1.23 a.u.) and krypton (−1.41 a.u.). Thus, if sharp differences between experimental NSDI results for Xe and Kr were to appear, significant modifications to the smooth-core potentials of the TDNE approach would be mandated.

A TDNE advantage over laboratory experiments comes from the ability to accumulate a numerical record of every trajectory in the ensemble from beginning to end. This permits selection of interesting end results, for example, those that lead to NSDI versus those leading to single ionization or to SDI, and then to trace just those trajectories through all stages of evolution back to their initiations (Panfili, Eberly, and Haan, 2001; Haan *et al.*, 2002). This so-called back analysis is invaluable in building explanations for momentum distributions, for example, the distinctions corresponding to direct first-pass knockout of the inner electron versus a one-cycle or few-cycle delay before a successful collision occurs. Other distinctions arise between ionizations early or late in the pulse turn-on, and so on. This capability is most useful for TDNE analysis, and to an extent for TC analysis as well, but is not available in the FD approach.

Every classical NSDI event must start with an overbarrier escape of the first electron, since tunneling is classically forbidden. The laser field periodically and strongly suppresses the atomic potential such that one of the electrons may escape over the barrier easily. However, the smoothing parameter a of the shielded potential $V_{n,i}$ [cf. Eq. (16)] puts a lower limit on the quasi-Coulomb potential well and this prevents autoionization. Given the pair of actively interacting bound electrons, it is not difficult for one of them to steal a bit of energy from the other and promote itself out of the atom, as is evident in Fig. 7.

A series of snapshots of a completely classical NSDI event is shown in Fig. 8, taken at several times before and after a recollision has liberated the second one. Note the substantial localized distortions in the tilted potentials, one at the position of each electron, indicating the repulsive contribution each can make to the other's escape.

Positive attributes nearly exceptional to TDNE in addition to back analysis include the ability to treat triple and higher multiple ionizations. These are open to direct experimental examination, but cannot be treated by any FD or TDSE approaches. In Sec. VI.G, we compare the TDNE results for double and triple ionization of argon with experimental data. Also, general elliptical polarization can readily be dealt with nonperturbatively by TDNE, and in agreement with initial experimental reports (see Sec. VI.C). This is currently not feasible via the TDSE in any dimensionality.

C. SFA extension via Feynman-diagram modeling

While the TDSE wave function or the ensemble of TDNE trajectories is similar to a catalog containing all possible outcomes from a given initial state, the S matrix allows one to select any particular item from the catalog without having to order the whole book. That is to say, an S-matrix element is the transition amplitude into a given final state, which for NSDI is characterized by the laser vector potential $\mathbf{A}(t)$ and the momenta $\mathbf{p}_1$ and $\mathbf{p}_2$ of the two final electrons, and it can be calculated by itself. This is a significant advantage

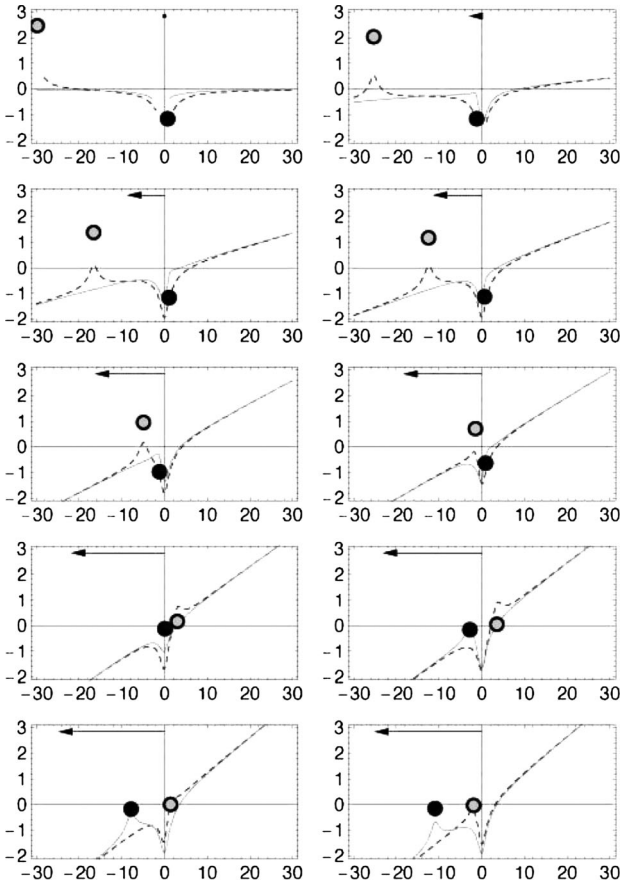

FIG. 8. Snapshots showing two-electron dynamics near the end of a double-ionization scenario, calculated in the aligned-electron approximation. In the first panel one electron (solid dot) is still deeply bound to the core, and the other has already been ejected and is returning from a far-left excursion under laser control, after it has been accelerated by the laser field during the preceding half cycle. It approaches, slowing down as it is now moving against the field and the laser potential rises, and collides in the fourth row with enough energy to liberate the other one, so that both exit together to the left in the last panel. The horizontal axis shows position and the vertical axis shows total energy, both in atomic units, while the arrow indicates the direction and strength of the laser field. The dashed and solid curves indicate the combined potential of nucleus, *e*-*e* repulsion, and laser field felt by the electrons, i.e., $V_{n,i}(x_i) + V_{ee}(x_{12}) + x_i E(t)$ as a function of x_i, with the other electron being in the position indicated. The plots extend over slightly more than a quarter cycle. Time increases from left to right and from top to bottom, as illustrated by the arrow that specifies the electric field. From Panfili, Haan, and Eberly, 2002.

whenever the corresponding transition amplitude is very small so that the wave function would have to be evaluated with very high accuracy or the ensemble of TDNE trajectories would have to be very large in order to contain a few representatives of the process.

An exact evaluation of the S matrix, which amounts to an exact solution of the quantum-mechanical two (or more) particle breakup problem with an external time-dependent force, is, of course, completely out of reach. Next we review a quantum-mechanical step-by-step approach to approximate the S matrix, which extends the SFA of Sec. II.B to double ionization.

The contributions to a perturbative expansion of the S matrix can be efficiently represented by Feynman diagrams. Feynman-diagram modeling is based on separating the Hamiltonian (4) into a part that is, at least in principle, treated exactly while the remainder is completely neglected or dealt with perturbatively to lowest order. We write

$$H = H_0 + H_A(t) + H_B(t), \tag{17}$$

where H_0 is the free two-electron Hamiltonian, and the five interaction terms of the full Hamiltonian are arranged into $H_A(t)$ and $H_B(t)$. The two interactions with the laser field are explicitly time dependent. The exact time-evolution operator $U(t, t')$ of the complete Hamiltonian H satisfies the integral equation

$$U(t, t') = U_{0A}(t, t') - i \int_{t'}^{t} dt'' U(t, t'') H_B(t'') U_{0A}(t'', t'), \tag{18}$$

where $U_{0A}(t, t')$ is the time-evolution operator of the Hamiltonian $H_{0A}(t) = H_0 + H_A(t)$. The second term on the right-hand side can also be written in the opposite order $U_{0A}(t, t'')H_B(t'')U(t'', t')$. Iteration of the integral equation (18) allows us to follow the time evolution generated by $H_{0A}(t)$ exactly while taking account of $H_B(t)$ perturbatively. At different stages of the double-ionization process, different partitions are taken as appropriate.

This partition method has been dubbed "intense-field many-body S-matrix theory"; see Becker and Faisal (2005) for a review. It does not itself suggest one unique expansion of the S matrix. Rather, it requires that one have in mind a particular scenario of how double ionization proceeds. Figure 9 exhibits the two examples that we discuss in this review, namely, the RII scenario laid out above in Sec. II.C as well as recollision excitation with subsequent ionization

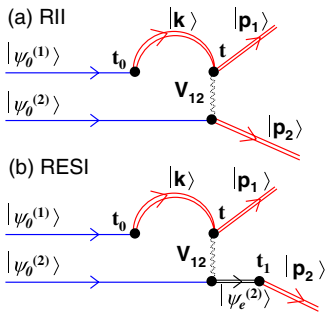

FIG. 9 (color online). (a) The Feynman diagram proposed by Kuchiev (1995) and by Becker and Faisal (1996) that describes the quantum SFA amplitude (20), which implements the recollision–impact-ionization (RII) pathway, which is the Corkum recollision scenario. Time goes from left to right. The single lines represent the two electrons in their initial field-free bound states. Double lines represent electrons interacting with the field but not with the ion or each other (Volkov states). The vertical wavy line stands for the *e*-*e* interaction V_{ee} (labeled V_{12}). (b) Diagram that describes the recollision-excitation and subsequent ionization (RESI) pathway: in the *e*-*e* interaction, the second electron is promoted into an excited bound state $|\psi_e^{(2)}\rangle$, from which it tunnels out at the later time t_1. From Figueira de Morisson Faria and Liu, 2011.

(RESI). These two scenarios appear to be the most important under the conditions of current experiments. The Feynman diagram for a shake-off process was also identified and evaluated and deemed to be irrelevant under current Ti:sapphire laser conditions (Becker and Faisal, 2002). These remarks also recall to mind the main conceptual distinction between the FD approach and the previously described TDSE and TDNE approaches, since neither of the latter alter their calculations depending on imagined interaction sequences.

The partitions that implement the RII scenario are the following. The initial state is the field-free two-electron atom, so $H_0 + H_A(t)$ describes the two-electron atom in the absence of the laser field while the interaction with the laser field is relegated to $H_B(t)$. In the final state, both electrons predominantly interact with the laser field so that $H_A(t) = H_0 + (\mathbf{r}_1 + \mathbf{r}_2) \cdot \mathbf{E}(t)$, and the final state is the product of two Volkov states (6), one for each electron. In the intermediate stage, the two electrons are considered on unequal footing such that one (electron 2) propagates bound to the nucleus while the other (electron 1) is free and only interacts with the laser field. In this case, we take $H_A(t) = V_{n,2}(\mathbf{r}_2) + \mathbf{r}_1 \cdot \mathbf{E}(t)$, while the remaining interactions are included into $H_B(t) = V_{n,1} + \mathbf{r}_2 \cdot \mathbf{E}(t) + V_{ee}$. The propagation of electron 1 is governed by the Volkov propagator

$$U_{\mathrm{V}}(t, t_0) = \int d^3\mathbf{k} \, |\psi^{\mathrm{V}}_{\mathbf{k}}(t)\rangle\langle\psi^{\mathrm{V}}_{\mathbf{k}}(t_0)|, \tag{19}$$

which can be constructed from the Volkov functions (6) as shown. With time going from left to right, these three stages are reflected in the Feynman diagram depicted in Fig. 9.

The procedure just outlined gives rise to the formal expression

$$S_{\mathbf{p}_1\mathbf{p}_2} = -\int_{-\infty}^{\infty} dt \int_{-\infty}^{t} dt_0 \{\langle\psi^{\mathrm{V}}_{\mathbf{p}_1}(t)| \otimes \langle\psi^{\mathrm{V}}_{\mathbf{p}_2}(t)|\} \times V_{ee} U_{V1}(t, t_0) V_{n,1} \{|\psi_0^{(1)}(t_0)\rangle \otimes |\psi_0^{(2)}(t)\rangle\}, \tag{20}$$

where $U_{V1}(t, t_0)$ indicates the Volkov time-evolution operator for electron 1. For further details of the derivation of the amplitude (20) see Becker and Faisal (2005). Differently motivated derivations of essentially the same result were given by Kuchiev (1995, 1996) and by Kopold *et al.* (2000). Note that Eq. (20) and the same with $V_{n,1}$ replaced by $\mathbf{r}_1 \cdot \mathbf{E}(t_0)$ are equivalent, as can be shown by an integration by parts [see, e.g., Becker *et al.* (2002)]. Both forms have been used.

The physical content of the amplitude (20) becomes especially clear from the Feynman diagram of Fig. 9, which is similar to a graphical representation of the recollision model. We note that the electron-electron interaction V_{ee} is crucial, because it is via this interaction that the returning electron is able to dislodge the bound one. In general, the amplitude (20) shares with the single-ionization SFA its defining properties: neglect of the effect of the laser field on the initial state as well as that of the binding potential on the final state, by using the Volkov state $|\psi^{V}_{\mathbf{p}}(t)\rangle$ in Eq. (6) for the latter, and neglect of the laser force on the second electron before the recollision.

In principle, the S-matrix element (20) should start from the fully correlated ground state $\langle\mathbf{r}_1, \mathbf{r}_2|\Psi_0(t)\rangle$ (for helium) instead of the product $|\psi_0^{(1)}(t)\rangle \otimes |\psi_0^{(2)}(t)\rangle$ of the one-electron ground states of the neutral and the singly ionized atom. In principle, it should also allow the singly ionized atom to be in an excited state after the first electron has tunneled into the continuum. However, both of these complications were assessed only to have a minor quantitative effect (Becker and Faisal, 1996) and have been dropped since. The single-electron ground states $|\psi_0^{(i)}\rangle$ have been approximated differently in different calculations (Figueira de Morisson Faria and Lewenstein, 2005).

Equation (20) formalizes the RII scenario. There are many other possible scenarios that contribute to the given S-matrix element, which proceed via collective tunneling (cf. the end of Sec. II.C), via shakeup (the first electron on its way out distorts the ion so that a second electron is ejected), or via other scenarios. In principle, all of these would appear in a systematic expansion of the S-matrix element. The most important additional scenario that has been developed extensively is the RESI pathway, illustrated in Fig. 9(b), which requires one additional iteration of the integral equation (18). The result has three temporal integrations: one over the time when the first electron is ionized, the second over the time when it recollides and promotes the still-bound electron 2 to an excited state, and the third over the time when this electron leaves the excited state via tunneling. We refrain from writing down the formal expression (Kopold *et al.*, 2000; Shaaran, Nygren, and Figueira de Morisson Faria, 2010) and just exhibit the Feynman diagram in Fig. 9(b).

The FD amplitude (20) as it stands involves two temporal integrations and two over space (each three dimensional). Straightforward integration requires Monte Carlo techniques and is very time consuming. A different procedure has proved advantageous: first one expands the Volkov time-evolution operator $U_{\mathrm{V1}}(t, t')$ in terms of the Volkov wave functions (6) as shown in Eq. (19), which introduces an additional integration over the drift momenta $\mathbf{k}$ of the latter. Since the Volkov wave functions are (time-dependent) plane waves, the spatial integrations now yield Fourier transforms of the interaction and the binding potentials, that is, "form factors." The potentials are chosen (in effect by making an *ad hoc* modification of the ionic core) such that these can be carried out analytically. For strong laser fields, the rapid exponential time dependence of the Volkov wave functions (6) calls for an evaluation of the remaining integrals over $\mathbf{k}$, t, and t_0 by the method of steepest descent (Lewenstein *et al.*, 1994). The procedure has been laid out in detail by Figueira de Morisson Faria, Liu, Schomerus, and Becker (2004); Figueira de Morisson Faria, Schomerus, Liu, and Becker (2004); see also Figueira de Morisson Faria and Liu (2011).

The saddle points $(t_s, t_{0s}, \mathbf{k}_s)$ $(s = 1, 2, \ldots)$, which depend on the final momenta $\mathbf{p}_1$ and $\mathbf{p}_2$, define classical electron trajectories: an electron is set free at time t_0 at the position of the ion with zero velocity, acquires the drift momentum $\mathbf{k}$, revisits its parent ion at the time t, and dislodges the second bound electron, whereupon both continue to travel in the laser field with drift momenta (final momenta) $\mathbf{p}_1$ and $\mathbf{p}_2$. We mention that the saddle points, especially the tunneling time t_0, and in turn the corresponding trajectories involve a subtlety: they have nonzero imaginary parts. This reflects their quantum-mechanical origin through tunneling and is

well known in the description of tunneling processes (Hauge and Støvneng, 1989). These so-called "quantum orbits" have become a powerful tool in the theory of intense-laser-atom processes (Salières *et al.*, 2001), which conveys an intuitive picture of how the processes develop in time. Their application to NSDI has been demonstrated by Figueira de Morisson Faria and Becker (2003). Even though the orbits are much simpler, they can be compared with the TDNE trajectories. Compare, for example, Fig. 7 with the rescattering quantum orbits of Fig. 6 of Kopold, Becker, and Kleber (2000).

Interference effects between different orbits provide a significant fundamental difference between the FD and the TDNE results; see Figueira de Morisson Faria and Becker (2003) and, for a very intriguing manifestation involving many orbits, see Popruzhenko *et al.* (2002). However, interference effects have not yet been observed in experiments, except possibly in NSDI of molecules (see Sec. VI.E). One reason is that the experimental yield of NSDI data is not high enough to allow for a fully differential analysis so that some components of the six-dimensional space of the final momenta $\mathbf{p}_1$ and $\mathbf{p}_2$ are always integrated over, which tends to smear out interference effects. The fact that experiments always imply some focal averaging has the same consequence. Another purely quantum feature is tunneling, but it does not appear to leave a clear signature. This can be concluded from comparison with TDNE results (Ho, Liu, and Becker, 2007).

The quantum elements in the amplitude (20) then are (i) tunneling as expressed in the fact that the ionization time is complex, (ii) interference of the various solutions of the steepest-descent equations, and (iii) quantum spreading of the electronic wave packet between ionization at time t_0 and recollision at time t, which is accounted for by the time-evolution operator $U_V(t, t_0)$.

A modification of FD theory has been proposed in which the quantum features (ii) and (iii) are dropped. The resulting expression for the transition rate is (Figueira de Morisson Faria, Liu, Schomerus, and Becker, 2004; Figueira de Morisson Faria, Schomerus, Liu, and Becker, 2004)

$$F(\mathbf{p}_1, \mathbf{p}_2) = \int dt_0 w(t_0) \delta\Big(\sum_{i=1}^{2} \frac{1}{2}[\mathbf{p}_i + \mathbf{A}(t)]^2 + I_{\mathrm{P2}} - E_{\mathrm{ret}}(t)\Big) |V_{\mathbf{p}-\mathbf{k}}|^2. \tag{21}$$

Similar to the quantum-mechanical amplitude (20), this is an integral over the ionization time t_0, but here the recollision time t is a function of t_0 and is calculated via classical simpleman mechanics (Corkum, 1993; Kulander, Schafer, and Krause, 1993), assuming that the first electron is set free with zero velocity at the time t_0; cf. Sec. II.C.

The distribution function (21) incorporates the three steps of the RII scenario incoherently (multiplicatively). Tunneling is specified by the rate $w(t_0)$, and propagation from the ionization time t_0 to the recollision time t determines the kinetic energy $E_{\mathrm{ret}}(t)$ of the returning electron. Finally, inelastic recollision is subject to energy conservation (expressed by the δ function) and the momenta are distributed according to the square of the form factor $V_{\mathbf{p}-\mathbf{k}}$, which is the Fourier transform of the e-e interaction V_{ee} where $\mathbf{p} = (\mathbf{p}_1, \mathbf{p}_2)$ and $\mathbf{k}$ is the drift momentum of the returning electron, also to be calculated from classical mechanics (Figueira de Morisson Faria, Liu, Schomerus, and Becker, 2004; Figueira de Morisson Faria, Schomerus, Liu, and Becker, 2004). The classical boundaries of the ion-momentum distribution and the electron momentum-momentum correlation have been estimated by Pohl, Ebeling, and Romanovsky (2003) and Milošević and Becker (2003).

Even though the transition rate (21) combines only classical ingredients except for the initial tunneling stage, it is still similar to an S matrix, because first the initial state and the final electron momenta $\mathbf{p}_1$ and $\mathbf{p}_2$ are specified and then the corresponding transition rate is calculated.

A crucial ingredient of the recollision scenario is the electron-electron interaction potential V_{ee} by which the returning electron kicks out the second electron. In the FD calculation, this potential enters only in first-order Born approximation. Of course, the standard Coulomb repulsion potential

$$V_{ee}(\mathbf{r}_1, \mathbf{r}_2) = \frac{1}{|\mathbf{r}_1 - \mathbf{r}_2|} \tag{22}$$

appears as the natural choice (Becker and Faisal, 1996, 1999a, 2000, 2002; Goreslavski and Popruzhenko, 2001; Goreslavskii *et al.*, 2001; Popruzhenko and Goreslavskii, 2001; Weckenbrock *et al.*, 2003), but the contact potential

$$V_{ee}(\mathbf{r}_1, \mathbf{r}_2) = V_0 \delta(\mathbf{r}_1 - \mathbf{r}_2)\delta(\mathbf{r}_2) \tag{23}$$

has been frequently used (Kopold *et al.*, 2000; Goreslavskii *et al.*, 2001; Figueira de Morisson Faria, Liu, Sanpera, and Lewensein, 2004; Figueira de Morisson Faria, Liu, Schomerus, and Becker, 2004; Figueira de Morisson Faria, Schomerus, Liu, and Becker, 2004). It is, actually, a three-body potential since for this potential to act it is not sufficient that the two electrons are at the same position, but this position must be the position of the ion (which is located at the origin). Recalling the various approximations and limitations inherent in the SFA and built into the amplitude (20) one need not hesitate to consider the e-e interaction V_{ee} as an *effective* interaction.

It is a major challenge to improve the SFA-FD method by including more of the many interactions that are unaccounted for and this is typically done on an *ad hoc* basis. The Coulomb repulsion between the two electrons in the final state can comparatively easily be taken care of with the help of the two-electron Volkov solution developed by Faisal (1994). However, the results do not really lead to better agreement with the data (Figueira de Morisson Faria, Liu, Schomerus, and Becker, 2004; Figueira de Morisson Faria, Schomerus, Liu, and Becker, 2004). It is much more difficult to accomplish a better description of the electron-ion interaction. This was attempted by utilizing the strong-field eikonal Volkov approach (Smirnova, Spanner, and Ivanov, 2008) by Bondar, Liu, and Ivanov (2009) for intensities below the recollision threshold (cf. Sec. VI.A), but the resulting momentum distributions are much narrower than in the data.

D. Tunneling-classical trajectory methods

In contrast to the fully classical TDNE approach, the TC trajectory approach retains electron tunneling as the initiator

of the NSDI process, which is then followed by classical electron trajectory propagation. In this way it is similar in spirit to the Corkum (1993) recollision model of NSDI. However, it goes beyond that in the sense that all interactions are engaged after the first step of tunneling, just as in the TDNE approach. Conceptually, the model envisions NSDI to be generated by two important processes, which are treated separately and sequentially: quantum-mechanical tunneling followed by a classical trajectory propagation (we refer to this model by the tunneling-classical acronym TC). This is, of course, a model assumption. There is no known way to tell at which exact instant tunneling is completed and classical propagation starts.

The TC approach shares with the TDNE model all of those features that are relevant, but only after the tunneling event. All five of the participating interactions that we mentioned are considered fully and equally. TC calculations can be performed for a broad range of laser parameters, such as wavelength, intensity, pulse shape, and polarization, always under the provision that the picture of tunneling ionization still holds. The TC model also allows one to identify those individual NSDI trajectories that lead to NSDI and to back analyze the pertinent dynamics in all details.

The acronym TC may also be used to subsume a step-by-step approach that models the various steps separately, trying to incorporate the available field-free cross sections and paying constant attention to the significance of the Coulomb interaction (Yudin and Ivanov, 2001a). The model especially predicts (Bhardwaj *et al.*, 2001) that the ratio of doubly to singly charged helium increases with pulse length and produces good agreement with corresponding data of Walker *et al.* (1994).

The TC as well as the FD approach needs to introduce I_P values by hand. It is only via the TDSE, and only for helium, that one has been able to deal with target atoms from first principles. The FD and the TC approaches, on the one hand, and the TDNE, on the other hand, differ in the amount of atom-specific input that enters them. For example, for double ionization the TDNE approach requires one only to specify the total ionization potential $I_{P1} + I_{P2}$. In contrast, in the FD and in the TC approach one separately has to specify both the first and second ionization potentials. Results will be very different depending on specific I_P values. Excited states do not directly enter either the TDNE or TC models.

The TC approach was initially used to explore the effect of Coulomb refocusing on the double-ionization yield (Brabec, Ivanov, and Corkum, 1996). Extensive investigations of the NSDI dynamics with the TC method (Chen *et al.*, 2000; Fu *et al.*, 2001; Chen and Nam, 2002; Fu, Liu, and Chen, 2002) were carried out after the differential data measured with COLTRIMS had become available in the early 2000s. The laser pulse is assumed to be at full strength at the time of tunneling, so the envelope function $E_0(t)$ is usually taken to have a constant amplitude for the first several cycles and then to turn off with a $\cos^2$ envelope within the last few cycles.

In order to perform the electron trajectory propagation according to Newton's equation of motion (14), the initial phase-space distribution of both electrons must be set up as in the TDNE model. The first electron is assumed to tunnel through the field-lowered Coulomb barrier and its initial conditions are determined by its wave function at the tunneling time t_0 (Landau and Lifshitz, 1977; Ammosov, Delone, and Kraĭnov, 1986). With the laser polarization in the x direction, the initial positions for the first electron are $y(t_0) = z(t_0) = 0$ while $x(t_0)$ is determined by the solution of $xE(t_0) - V_{n1} = I_{P1}$, where V_{n1} denotes the potential between the first-ionized electron and the singly charged ion, which is the same as employed in the FD approach [Eq. (20)], but not necessarily as the potential in TDNE [Eq. (16)]. The initial velocities of the first electron are set to $v_x = 0$, $v_y = v_\perp \cos\theta$, and $v_z = v_\perp \sin\theta$. For the tunneling rate $w(t_0)$ one usually uses the quasistatic tunneling rate (8) (Ammosov, Delone, and Kraĭnov, 1986).

The weight of each classical trajectory in the ensemble is evaluated by $w(t_0, v_\perp) = w(t_0)g(v_\perp, t_0)$. The quantum-mechanical transverse velocity distribution is

$$g(v_\perp, t_0) = (1/\pi\delta v_\perp^2)\exp[-(v_\perp^2/\delta v_\perp^2)], \tag{24}$$

where $\delta v_\perp = [|E_0(t_0)|/\sqrt{2I_{P1}}]^{1/2}$ (Delone and Krainov, 1998). For the simulation, values of $v_\perp$ up to several times $\delta v_\perp$ are typically chosen. The time t_0 is varied over the first optical half cycle. The initial conditions of the second electron are determined by assuming that the electron is in the ground state of the singly charged ion and its initial phase space is modeled by a microcanonical distribution.

To find double-ionization events, Eq. (14) is solved in a time interval from t_0 until the end of the pulse. If both electron energies are greater than zero at the end of the laser pulse, a double-ionization event has taken place.

It should be noted that, while the initiation by tunneling ionization in the TC method has not yet resulted in any qualitatively distinct NSDI features compared with the TDNE results, it may give rise to some nontrivial aspects in the calculation procedure, which deserve to be mentioned. For example, autoionization, which in the TDNE model has to be prevented by adopting the softened potentials (16), is of no concern, in principle, in the TC model owing to the tunneling initiation of the trajectories. Therefore, the potentials can be exactly taken as

$$V_{n,i} = -\frac{Z_{\text{eff}}}{r_i}, \tag{25}$$

where Z_{eff} is the effective charge of the singly charged ion. Only for helium does its value equal 2, while for the other atomic species it can be derived from the ionization potential I_{P2} of the singly charged ion. For the e-e potential, the unscreened Coulomb potential (22) is adopted.

If one intends to extend the TC model to multiple (triple or higher) ionization, one needs to set up an initial phase space for the two (or more) bound electrons by a microcanonical distribution, as is commonly done for NSDI in the TDNE model. The problem of autoionization, as encountered in the TDNE model, then has to be considered and one is forced to employ softened potentials; see Sec. VI.G.

In the TC model, usually only the tunneled electrons produced in the first half cycle of the pulse are traced to obtain the results. Also, the depletion of the ground state has not been considered. Regarding the many-cycle pulses employed in experiments, one might ask whether this simplification may lead to some deviation of the TC results from the

data. In fact, this does not seem to be a problem when the laser field intensity is not too high and the concept of tunneling ionization can still be justified. However, ground-state depletion must be considered if the laser intensity increases further such that the over-barrier-ionization regime is reached. Also, the assumption of tunneling to initiate NSDI becomes questionable in the over-the-barrier regime. Note that the sudden turn-on of the field, which has been assumed in the TC model, rules out effects to be discussed for elliptical polarization in Sec. VI.C.

The model underlying Eq. (21) of Sec. IV.C conceptually resembles the TC model, in the sense that it involves quantum tunneling followed by completely classical simpleman propagation. Otherwise, however, it is so similar to the spirit and the assumptions of the quantum FD model that we have considered it in that context.

As a final example of the TC approach, we mention the classical analysis by Sacha and Eckhardt (2001a) of two electrons, which are driven by the laser field through the saddle in phase space on the equipotential surface formed by the three Coulomb potentials. The subspace of symmetrically escaping electrons generates the double-hump distribution of the doubly charged ion. Only the last step of NSDI is investigated: the process of electron excitation to the excited state that precedes this classical motion is taken for granted and not analyzed. The model has been extended to triple ionization (Sacha and Eckhardt, 2001b). The motion across the saddle was also formulated quantum mechanically (Prauzner-Bechcicki *et al.*, 2008).

V. COMPARISONS OF THEORY WITH EXPERIMENT

Comparison of data with theoretical predictions serves to identify successes and failures in theoretical modeling when fundamental theoretical principles cannot be followed to the end, as is ultimately almost always the case.

A. Doubly charged ion-yield measurements: The knee

To begin, one sees in Fig. 10 that several different approaches can capture the signature element of NSDI, the knee feature, in their ion-count predictions. This is a strong indication of the fundamental character of the new physics evident in the knee, i.e., the existence of strong two-electron correlation effects in this high-field ionization domain.

Referring to Fig. 10, and taking each row in turn, a knee showing the same form as the data of Fittinghoff *et al.* (1992) is shown in the top left as calculated by Corkum (1993) and included in his seminal paper that proposed the rescattering model. Corkum's calculation utilized as input the Ammosov-Delone-Kraĭnov (ADK) ionization rate (Ammosov, Delone, and Kraĭnov, 1986), the known $(e, 2e)$ cross section for He^+, and an estimate of the width of the recolliding electron's wave packet. Next are shown excellent fits to data resulting from an *ad hoc* approach to the TDSE that allowed the outer electron to interact with the inner one, but not vice versa (Watson *et al.*, 1997). This was essentially a formal implementation of inelastic rescattering. In the second row of Fig. 10 we show that the yield versus intensity curves for the whole gamut of data available for helium in the late 1990s was remarkably

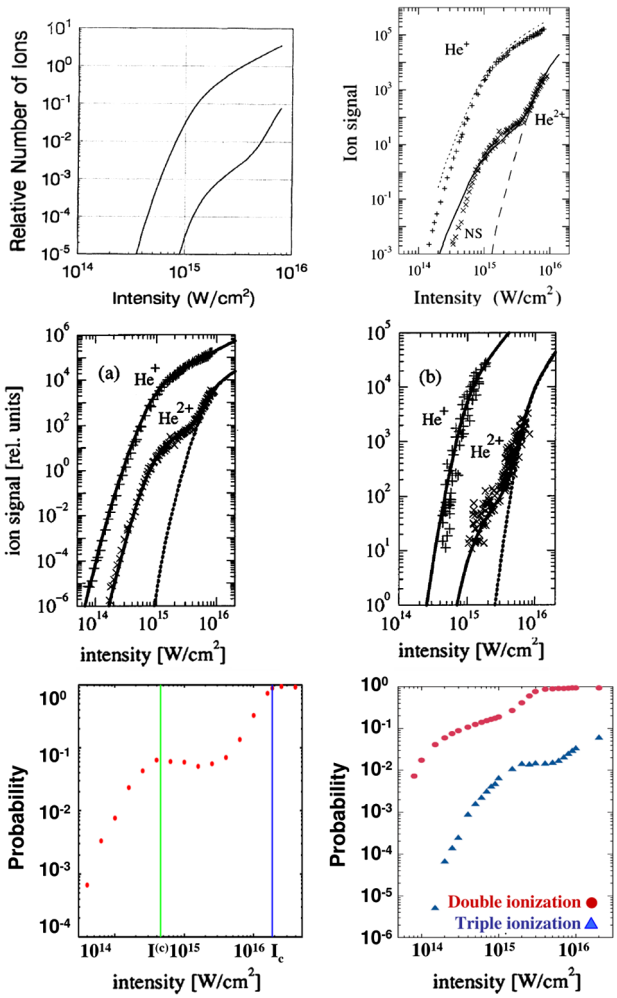

FIG. 10 (color online). The ability of a wide variety of NSDI theories demonstrated to recover the signature knee effect. From the top left they are taken from Corkum (1993), Watson *et al.* (1997), Becker and Faisal (1999a), Mauger, Chandre, and Uzer (2009), and Ho and Eberly (2006) as discussed in the text.

well reproduced by a model formula for the nonsequential-double-ionization rate (Faisal and Becker, 1997; Becker and Faisal, 1999a) that was motivated by the Feynman diagram of Fig. 9, but drastically simplified in order to allow for evaluation within a reasonable amount of computer time and adaptation to atoms other than helium. These first four graphs can all be understood as results from the step-by-step approach.

Knees have also been calculated using the all-at-once approach, as shown in the last row of Fig. 10. Here a different goal is to be understood: one is not so much interested to show how to match experimental data closely, but rather to determine whether or not such a novel feature as a knee can actually emerge under steady action of the full combination of forces at work on the two electrons from the laser, the nucleus, and each other, without *ad hoc* timing sequences or equation modifications. The answer is again positive and positive from several points of view. First, the TDNE and TC calculations show knees based on the full two-electron theories described. Second, the same is true of a quite different all-at-once approach coming from classical phase-space

analysis (to be elaborated on in Sec. VI.D). Third, the last graph (Ho and Eberly, 2006) shows a theoretical knee that is more realistic than any others completed so far in the sense that the calculation included three electrons, all three equally active. Without imposing any ordering of ionization events on the electrons, this TDNE calculation produced a knee not only in double ionization but simultaneously in the triple-ionization data as well. We discuss nonsequential multiple ionization further in Sec. VI.G.

The all-at-once approach can be adjusted to any particular laser pulse shape desired, at least in principle, provided the pulse is not prohibitively long, and the result can immediately be compared with the experiment to which the calculation was tailored. In contrast, FD calculations are mostly carried out for an infinitely long monochromatic pulse and will, therefore, produce a double-ionization *rate*. Rate equations must then be used to obtain the yield of doubly charged ions for the pulse in question. They involve, as functions of time, the number of neutral atoms and singly and doubly charged ions and depend on the double-ionization rate as well as the single-ionization rates from the neutral atom to the singly charged ion and from the latter to the doubly charged species. It is useful to remark that there is no such thing as a *double-ionization rate for sequential ionization*. The yield for a sequential process can be obtained only from the single-ionization rates via solution of the rate equations.

B. *Ab initio* (TDSE) theory and experiment: Helium

Helium provides the only conceivable meeting ground between *ab initio* theory and experiment. The ultimate goal, comparison near the wavelength of 800 nm most frequently used in experiments, has not been accomplished yet. However, in Figs. 11 and 12 we present results from the Belfast group for the shorter frequency-doubled wavelength of 390 nm (Parker *et al.*, 2006). The intensities I are just below the nominal threshold intensity for the classical rescattering scenario (that is, for $3.17U_P < I_{P2}$). For helium $I_{P2} = 54.4$ eV, which means $I < 1.2$ PW/cm^2.

There are no arbitrarily adjustable parameters nor any input values in the Belfast calculations. All spectroscopic features of helium are implicitly calculated. The accuracy depends on the spacing of finite-difference grid points δr. In practice, with standard settings (e.g., $\delta r = 0.25$ a.u.), energies of bound states, energies of doubly excited states, and lifetimes of autoionizing states show agreement with theoretical values to better than 0.01%, 0.1%, and 1%, respectively. The time propagator of the HELIUM code was designed to meet a requirement for unusually small integration truncation errors. A typical integration (Parker *et al.*, 2006) might, for example, find total relative NSDI yields of the order 10^{-8} or even 10^{-12}, constraining local truncation errors to considerably less than 1 part in 10^{12}. To achieve this, HELIUM uses an arbitrary-order Arnoldi propagator (Smyth, Parker, and Taylor, 1998). Arnoldi propagators have often demonstrated improved integration efficiency in the limit of high order even if small truncation errors are not a requirement.

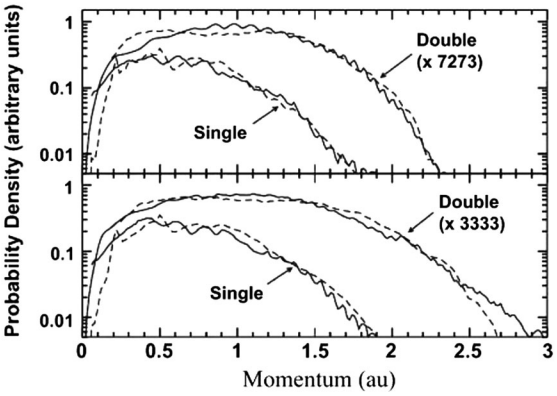

FIG. 11. Electron-momentum distribution for singly and doubly ionized helium at 390 nm and 0.8 PW/cm^2 (upper panel) and 1.1 PW/cm^2 (lower panel), experimental results (dashed curves) and TDSE (solid curves). For double ionization, the momentum of just one electron is plotted. From Parker *et al.*, 2006.

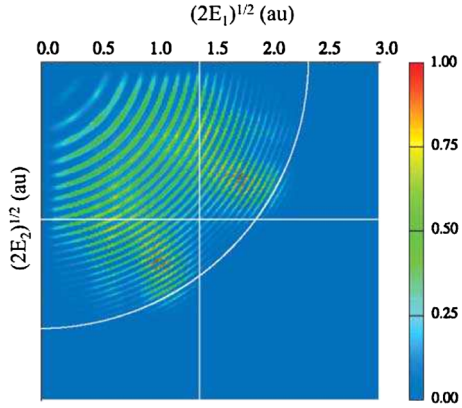

FIG. 12 (color online). TDSE calculation of the distribution of the momenta $p_i = \sqrt{2E_i}$ ($i = 1, 2$) of the two electrons emitted in double ionization at the end of a 7-period pulse with 1.0 PW/cm^2. The straight lines correspond to an apparent cutoff energy of $1.9U_P$ of the electrons coincident with single ionization. The circular arc is drawn at a total kinetic energy of $5.3U_P$ in order to serve as a cutoff for the total energy. From Parker *et al.*, 2006.

For comparison with experimental helium data from the DiMauro group see the two panels of Fig. 11, which exhibit measured and calculated electron-momentum distributions in coincidence with single as compared with double ionization. The agreement between theory and experiment is remarkable. The electron spectrum in single ionization is compatible with the cutoff at $2U_P$, which is expected from the simplest classical estimate (11), while the cutoff energy for an electron emitted in double ionization is substantially higher.

It is not currently feasible to obtain sufficient numerical data to permit detailed electron-ion and electron-electron momentum distributions for comparison with experimental data from helium, such as obtained via COLTRIMS. The running times for the numerical programs are simply too long. Additionally, there is no hope to extend this TDSE work to more complex atoms than helium, eliminating the chance to compare results with the richer data available particularly from the heavier noble-gas elements neon and argon. For the same reason, TDSE progress to more than two active electrons, mandatory for triple and higher nonsequential ionization, now repeatedly observed in the laboratory, is out of the question barring conceptual breakthroughs in computation.

Figure 12 shows a calculated TDSE momentum-momentum correlation. Notice that this is for the absolute values $|\mathbf{p}_1| \equiv p_1 = \sqrt{2E_1}$ and $|\mathbf{p}_2| \equiv p_2 = \sqrt{2E_2}$ of the two electrons, in contrast to the correlation in Fig. 5, which is for the longitudinal momentum components $p_{1\|}$ and $p_{2\|}$. Hence, the plot in Fig. 12 provides no information about the direction in which the electrons are emitted. The figure displays several features worth mentioning. First, the population is concentrated on arcs, which correspond to the number N of photons absorbed from the laser field, cf. Eq. (1), so that $E_1 + E_2 = (p_1^2 + p_2^2)/2 = N\omega - I_{P1} - I_{P2} - 2U_P$. The dominance of the arcs confirms that the electrons really stem from NSDI events (sequential double ionization would not generate arcs but a distribution of grid points). Moreover, the discreteness of the arcs betrays integer photon numbers, a quantum feature. Second, the distribution appears to be well contained within the white circular arc at an energy of $5.3U_P$. For intensities above the aforementioned threshold intensity, this cutoff rises to about $7U_P$. [Remarkably, such a cutoff was observed at 800 nm in early TC calculations by Chen, Liu, and Zheng (2002)]. Third, the clear notch along the diagonal can be attributed to Coulomb repulsion between the two electrons, which disfavors equal momenta.

Longitudinal and transverse ion-momentum distributions in helium were first measured by Weber *et al.* (2000b) at the Ti:sapphire wavelength of 800 nm; see also de Jesus, Rudenko *et al.* (2004). They are rather well reproduced by FD calculations based on the Feynman diagram of Fig. 9(a) (Becker and Faisal, 2000; Popruzhenko and Goreslavskii, 2001). Only the dip in the longitudinal ion-momentum distribution is somewhat exaggerated. This suggests a contribution of the RESI diagram of Fig. 9(b), which was not included in the calculation.

A related process of fundamental interest, although outside the scope of this review, is two-photon double ionization of helium. For a frequency below the second ionization potential (i.e. $\omega < 54.4$ eV) only the nonsequential (often called direct) pathway is open. Interest in this system has been renewed by the development of bright tunable short-wavelength sources, such as the free-electron laser facility FLASH; for recent results, see Kurka *et al.* (2010). The system is also eminently suitable for *ab initio* TDSE simulation; recent examples, which provide a listing of earlier references, include Palacios, Rescigno, and McCurdy (2009) and Pazourek *et al.* (2011).

C. Fingerlike structures

In the momentum-momentum correlation data, a striking "fingerlike" structure containing higher-energy electrons was reported by two groups in 2007 in their correlated electron momenta spectra from high-resolution COLTRIMS measurements (Rudenko *et al.*, 2007; Staudte *et al.*, 2007) of NSDI of helium. As shown in Fig. 13, it displays a characteristic notch or V-shaped suppression on the diagonal, which suggests Coulomb repulsion between the two electrons as its origin. This was confirmed in TC calculations by Ye, Liu, and Liu (2008), which we reproduce in Fig. 14, to be compared with Fig. 1 of Staudte *et al.* (2007). While Fig. 14(a) displays the complete result, in the other three panels various

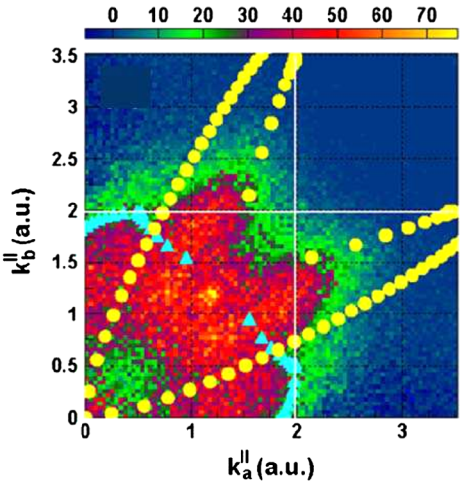

FIG. 13 (color online). First quadrant of the electron momentum-momentum correlation for NSDI of helium at 4.5×10^{14} W/cm^2 and 800 nm. The lines specify momenta of $2\sqrt{U_P}$. The triangles and circles present the kinematical boundaries obtained from a simple classical $(e, 2e)$ model. Namely, the recolliding first-liberated electron donates the energy corresponding to the second ionization potential to the second electron, which appears in the continuum with zero kinetic energy and is then accelerated by the field. In the process, the first electron either backscatters (dots) or forwardscatters (triangles). From Staudte *et al.*, 2007.

interactions are turned off or modified. In Fig. 14(b) the laser field is switched off and, indeed, the laser-induced drift (11) is absent; in Fig. 14(c) the e-e Coulomb interaction is replaced by a Yukawa interaction and, indeed, the V-shaped pattern is no longer present; and in Fig. 14(d) the electron-ion interaction is shielded, which greatly reduces the number of high-energy electrons.

Staudte *et al.* (2007) also exhibit TDSE calculations using the (2 + 1)-dimensional approach of Ruiz *et al.* (2006), which also agree well with the data. Emmanouilidou

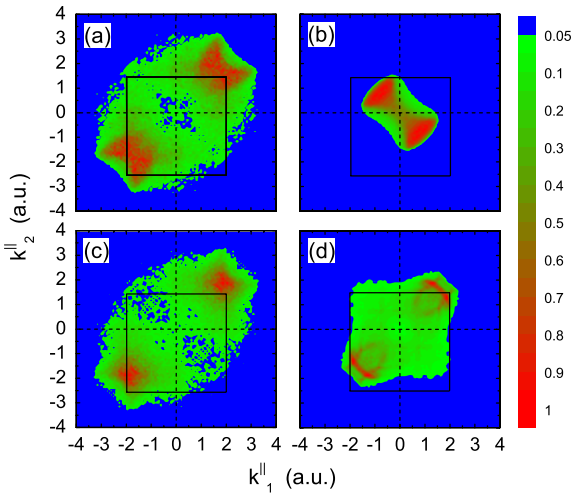

FIG. 14 (color online). Electron-electron correlations calculated from the TC model by Ye, Liu, and Liu (2008), intended to model the experiments of Rudenko *et al.* (2007) and Staudte *et al.* (2007). The laser intensity is 4.5×10^{14} W/cm^2 at 800 nm. See the text for further explanation and interpretation. From Ye, Liu, and Liu, 2008.

(2008), Haan, Van Dyke, and Smith (2008), and Ye, Liu, and Liu (2008) noticed that in order to obtain the fingerlike structure it may be imperative to take unscreened Coulomb potentials. With the softened electron-ion potential (16), the occurrence of hard electron-ion collisions is reduced. Since these generate the most energetic electrons, the yield of high-energy electrons may be to some extent weakened. Using unscreened Coulomb potentials within the TC approach, Xin, Ye, and Liu (2010) reproduced the fingerlike structure and investigated its dependence on the carrier-envelope phase (cf. Sec. VI.F). In principle, the V-shaped notch of Fig. 14 has the same origin as the one calculated *ab initio* by Parker *et al.* (2006) (see Fig. 12).

The data of Staudte *et al.* (2007) were also described in the context of a so-called quantitative rescattering theory (Morishita *et al.*, 2008), which is a phenomenological modification, designed to be more closely adaptable to specific atoms, of the quantum-mechanical rescattering theory [for a review of the latter, see Becker *et al.* (2002)]. The V-shaped notch is well reproduced if all three Coulomb interactions are taken into account (Chen, Liang, and Lin, 2010).

The V-shaped fingerlike suppression, evidently related to Coulomb repulsion, was already prominent in AEA TDSE simulations by Lein, Gross, and Engel (2000). A similar pattern can also be observed in (x_1, x_2) position space and clearly is also to be attributed to the same origin [Panfili, Eberly, and Haan (2001); recall Fig. 4].

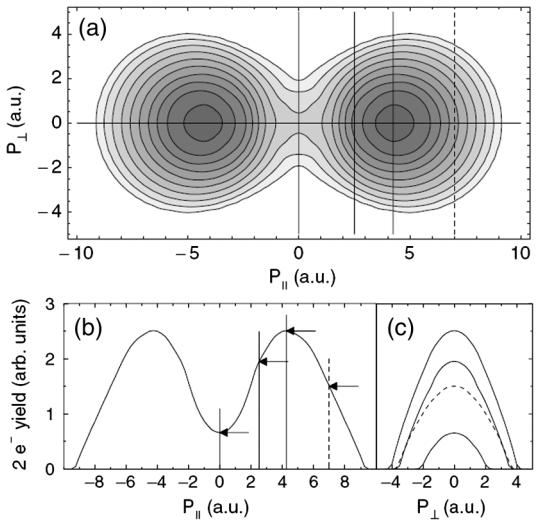

FIG. 15. Distribution of the ion momentum **P** in NSDI of neon at 795 nm calculated from the FD approach with zero-range interaction for all potentials, to be compared with Fig. 3. For a better simulation of the experiment, for the intensity the lower value 8×10^{14} W/cm^2 was taken. (a) Linear-scale density plot with ten equidistant contour lines. The horizontal line at $\mathbf{P}_\perp = 0$ and the four vertical lines at various values of $P_\parallel$ mark the positions of cuts along which the distribution is plotted in (b) and (c). From Kopold *et al.*, 2000.

D. Recollision–impact-ionization scenario: Neon

The COLTRIMS measurement of the momentum of the doubly charged neon ion reproduced in Fig. 3, whose distribution exhibits the typical double-humped shape, exhibited the footprint of the RII scenario. In Sec. III we confirmed that the positions of the centers of the two humps agree reasonably well with the simpleman estimate (11). The FD calculation of the distribution of ion momentum (negative sum of the two-electron momenta), carried out at an intensity lower than given in the experiment, is presented in Fig. 15. Both electron-ion interactions were described by contact potentials, and for the *e*-*e* interaction the three-body contact potential (23) was adopted. Comparison of Figs. 3 and 15 shows fair agreement in the distribution of the longitudinal ion-momentum component while the transverse widths of the distribution are considerably overestimated by the simulation, probably due to the fact that Coulomb refocusing is not included.

Figure 16(a) reproduces the electron-momentum correlation function for NSDI measured for neon (Moshammer *et al.*, 2003) replotted on the scale of $\sqrt{U_P}$. All plots display the double-ionization yield as a function of the momentum components parallel to the laser polarization direction, while the transverse components were not detected in the experiment and integrated over in the theory.

We first look at the experiment. The distribution of momenta is largely confined to the first and third quadrants. Each quadrant houses a roughly circular distribution with their centers at about $1.5\sqrt{U_P}$, somewhat below the simpleman value (11). There are very few events with momenta near zero or in the second or fourth quadrant. This is precisely what is expected from RII, which was already discussed in some detail in Sec. II.C.

Figures 16(b) and 16(c) present the results of TDNE calculations obtained in two or three spatial dimensions. The differences are minor (which can be invoked to justify restricting TDNE simulations to two dimensions). The centers of the distributions agree quite well with the experimental values. The TDNE distributions exhibit a slight minimum along the diagonal, which one is inclined to attribute to Coulomb repulsion between the two final electrons, which is not visible in the data of Fig. 16(a). Recall, however, that such a minimum was experimentally observed by Rudenko *et al.* (2007) and Staudte *et al.* (2007) for helium. It is also visible in the TC calculations shown in Fig. 14.

Figures 16(d) and 16(e) show results of pertinent FD calculations. Figure 16(d) reproduces the experimental result quite well, except for the positions of the two centers of the distribution, which correspond exactly to the simpleman value (11) rather than to the data. Figure 16(d) was obtained taking for the *e*-*e* interaction potential the three-body contact potential (23). The more reasonable Coulomb potential (22) leads to a distribution [Fig. 16(e)] that agrees less well with the experimental data. It is interesting to note that in the current case of rather high laser intensity, it makes practically no difference whether the calculation is based on the full quantum-mechanical amplitude (20) or on the classical expression (21) [the latter result is not shown here; cf. Figueira de Morisson Faria, Liu, Schomerus, and Becker (2004)]. This underlines the fact that the very simple physics that has entered the classical expression (21) is sufficient to explain the shape of the observed momentum-momentum correlation.

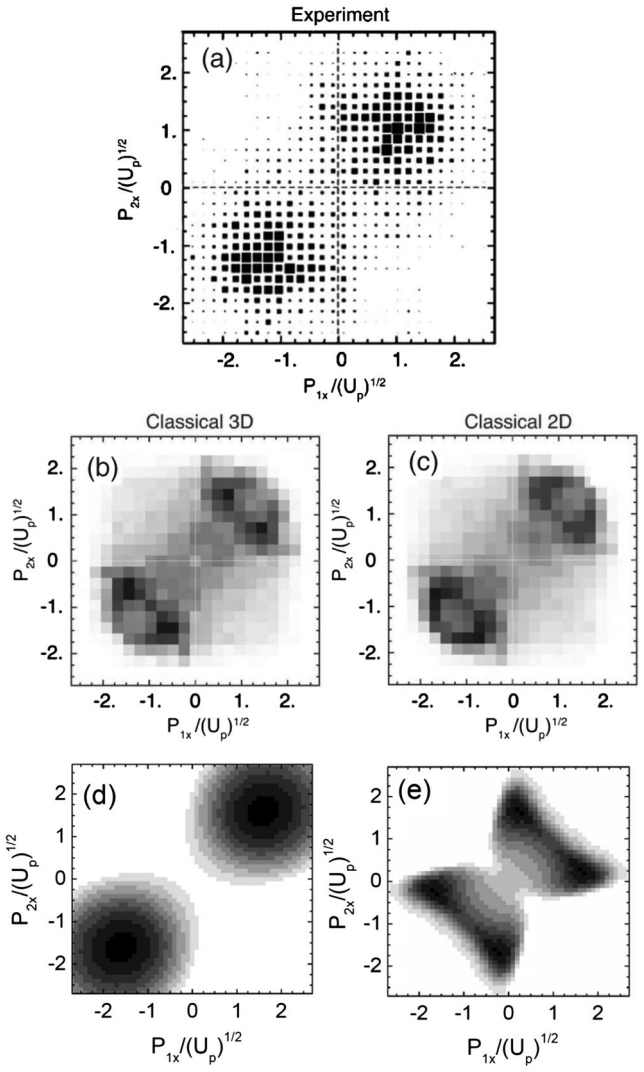

FIG. 16. Correlation function of the electron-momentum components parallel to the laser field for NSDI, plotted on the scale of $\sqrt{U_P}$, with the transverse components not measured (in the data) or integrated over (in the theory). (a) Measurements for neon at 1.0 PW/cm^2 and 800 nm [rescaled from Moshammer *et al.* (2003)]. Middle panels: three-dimensional (b) and two-dimensional (c) TDNE results for a two-electron "neon" atom exposed to a 780-nm 8-cycle trapezoidal laser pulse with an intensity of 0.3 PW/cm^2. The TDNE calculation is based on the analysis of more than 10×10^6 two-electron trajectories with the *e-e* smoothing parameter $b = 0.1$ in the Hamiltonian (4) [from Ho (2007)]. Lower panels: FD results computed from the *S*-matrix theory of Sec. IV.C for $\omega = 1.55$ eV, $I = 5.5 \times 10^{14}$ W/cm^2 ($U_P = 32.6$ eV), and the ionization potentials $I_{P1} = 21.5$ eV and $I_{P2} = 41$ eV corresponding to neon. The electron-electron interaction is modeled by the contact interaction (23) (d) or by the Coulomb interaction (22) (e). From Goreslavski *et al.*, 2001.

Figure 17 exhibits the momentum distribution of the doubly charged neon ion as measured [panel (c)] by Zrost *et al.* (2006) and compares it with the results of three-dimensional (left-hand column) and two-dimensional (middle column) TDNE computations. The second and third rows display the distributions of the longitudinal and one component of the transverse momentum, respectively. The experimental distribution is what one expects from Figs. 16(b) and 16(c): two well-separated humps, which are related to the momentum correlation being centered in the first and third quadrants. Note that the experimental data and the TDNE simulations are obtained at substantially different intensities; however, the results are scaled by $\sqrt{U_P}$. We notice that the results of the 2D and the 3D simulations differ mostly in the shape (cusp versus round top) and in the width of the transverse ion-momentum distribution. The two-dimensional distribution is wider. The reason is that the energy available for the transverse motion is the same in both cases. However, in the 3D case it is distributed over 2 rather than just 1 degrees of freedom. The 3D results agree quite well with the data. Especially, the position of the maxima is perfectly reproduced. Only the longitudinal width is slightly wider in the data.

E. The species dependence of NSDI

Already the first differential NSDI measurements revealed significant differences between different atomic species, especially between neon (Moshammer *et al.*, 2000, 2003), on the one hand, and helium (Weber *et al.*, 2000b) and argon (Weber *et al.*, 2000a, 2000c; Weckenbrock *et al.*, 2001; Moshammer *et al.*, 2002), on the other hand; cf. Figs. 3 and 5. For neon, under all conditions investigated below saturation, the ion-momentum distributions exhibit two well-separated humps and, correspondingly, the momentum-momentum correlations display predominantly side-by-side emission (population in the first and third quadrants) and a largely depleted region around zero momenta. In marked contrast, for helium and argon these features are less distinct or completely absent. The features just mentioned are the footprints of the RII scenario reviewed in Sec. IV.C. Hence, one cannot expect to see them if the conditions for this mechanism are not fulfilled. Especially, the maximal return energy $3.17U_P$ [Eq. (10)] of the recolliding electron must exceed the second ionization potential of the species. The first ionization potential for argon (15.8 eV) is substantially lower than for neon (21.6 eV). Therefore the saturation intensity is lower as well, and a sufficient return energy is harder to achieve.

However, these rather obvious considerations do not fully account for all of the NSDI data, in particular, for the differences existing between helium and neon, of which the former possesses a higher ionization potential (24.6 eV) than the latter (21.6 eV). Indeed, in addition to the RII mechanism, the contribution of the RESI mechanism [see Sec. IV.C and Fig. 9(b)] has been proposed to play a significant role in the species dependence of NSDI. This mechanism favors low-energy electrons, including also electrons emitted back to back. For argon at intensities below the RII threshold, such "anticorrelated" electrons actually become dominant (Liu *et al.*, 2010). It has also been argued that the ratio of the $(e, 2e)$ cross sections for ionization and for excitation is higher for neon than for argon (Feuerstein *et al.*, 2001; de Jesus, Feuerstein *et al.*, 2004; Herrwerth *et al.*, 2008) thereby favoring the RII pathway in the case of neon.

One-dimensional FD calculations were carried out for RESI, which indeed exhibited an increasing number of low-energy electrons (Kopold *et al.*, 2000) filling the gap that is left by the RII scenario. Recent three-dimensional

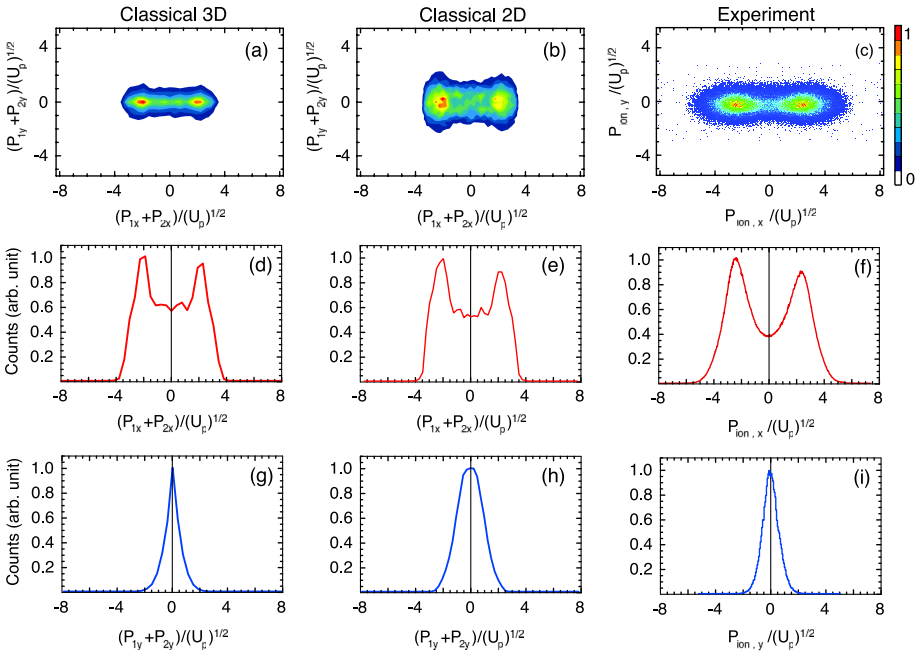

FIG. 17 (color online). Momentum distributions of the doubly charged neon ion from three-dimensional (left column) and two-dimensional (middle column) TDNE calculations and from the measurements of Zrost *et al.* (2006) (right column). The data were collected for a peak intensity of 1.5 PW/cm^2 at 795 nm, the intensity used for the simulations was 0.3 PW/cm^2. The uppermost row exhibits the two-dimensional ion-momentum distributions with one component not observed (in the data) or integrated over (in the 3D simulations). The middle row displays the distribution of the longitudinal momentum, and the lowermost row the distribution of the pertinent transverse component. From Ho, 2007.

computations (Shaaran, Nygren, and Figueira de Morisson Faria, 2010) showed that all four quadrants of the momentum-momentum correlation become populated, as expected.

Recently the TC approach was extended to account for the RESI pathway with a Wentzel-Kramers-Brillouin approximation employed to allow tunneling of the second electron (Ye and Liu, 2010). We return to this issue in Sec. VI.A. This extension sharpens the distinction between TC and TDNE approaches, since the latter only allows one to specify the sum of the first and second (for NSDI) ionization potentials, while the TC method depends on both. The interpretation of events as RESI events carries the implication that excitation is in fact happening prior to second ionization. A fully classical treatment has no excited states so a classical RESI interpretation has not been advanced in connection with TDNE calculations. However, approximately the same electron behavior could be obtained classically. This is based on the dual observation that (a) nothing in the dynamic multiforce TDNE calculations prevents excitation of the second electron while the first is ejected, and (b) even a quantum treatment should expect that under short-pulse wide-bandwidth pulses the second electron, when excited, is likely to find itself in a superposition of many closely spaced excited states, in close correspondence to a classical-like wave packet state, and not in an atomic bare state.

Finally, some TDNE results suggest a qualitatively attractive interpretation of momentum data based on striking features in energy trajectories of the type already shown in Fig. 7. In Fig. 18 one sees the stages of double ionization: (i) initiation, while the laser pulse is turning on and both electrons remain bound and are interacting strongly with each other, (ii) one electron has escaped but returns to the core one or several times, where various strong or weak interactions with the second still-bound electron take place, (iii) a strong enough collision occurs to cause a second ionization, and (iv) both ionized electrons oscillate widely in the laser field as they drift away from the core. Note that after ionization the electrons oscillate either in phase or exactly out of phase with each other, i.e., departing together to the same side of the ion or to opposite sides. These two possibilities correlate well with the delivery of momentum to the ion as noted by Ho and Eberly (2003). Essentially zero ion momentum (Z) is

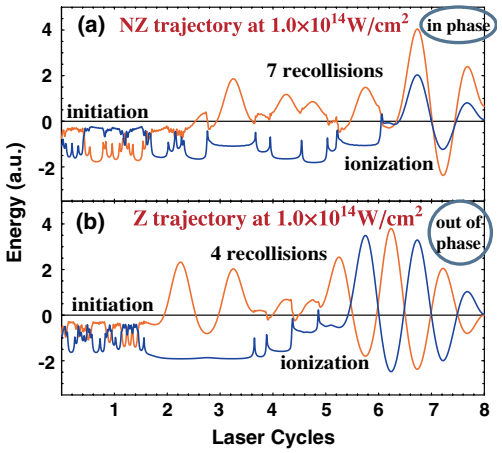

FIG. 18 (color online). Time evolution of the total energy, including dipole-interaction energy, of each NSDI electron during the first eight laser cycles. There are four clear stages of an NSDI process, as described in the text. From Ho *et al.*, 2005.

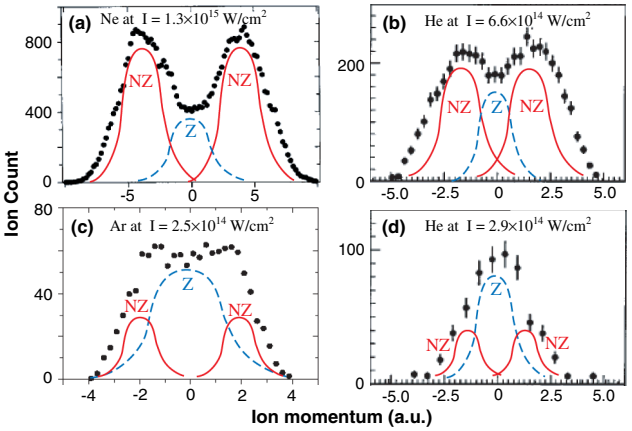

FIG. 19 (color online). COLTRIMS data from neon and argon are "matched" to TDNE results by hand, while full-blown TDNE calculations at two different laser intensities give similar results to the two helium panels, with an exaggeration of the Z contribution. From Ho *et al.*, 2005.

associated with oppositely directed departure trajectories, as in the lower panel of Fig. 18, and substantially nonzero ion momentum (NZ) is associated with codirected departures as in the upper panel.

The existence of two distinct momentum-production ionization events in these scenarios correlates surprisingly well with what appears experimentally as two distinct momentum distributions—those with two well-separated peaks and those with a central peak alone. An intermediate case, showing a filled-in center between two peaks, is also found. Examples of these three experimental results were given in Fig. 6. The TDNE interpretation of such data is shown in Fig. 19, where the Z and NZ scenarios are used to contribute as much of a two-peak or single-peak distribution as is needed to match the data. Thus what can be called a question about species dependence is turned into a question that asks what parameters of an atom and a laser pulse (e.g., pulse height and shape) are the ones that determine if ionization proceeds mostly as a Z or NZ process, or a combination. The TDNE approach has not addressed this question.

VI. CURRENT FRONTIERS OF NSDI

The wealth of new atomic features revealed by experimental high-field work on nonsequential double ionization has captured the attention of atomic, molecular, and optical physicists around the world. New questions have been raised and are beginning to be investigated. In this section we provide a short overview of some of them to highlight routes that have been opened for exploration. One clear path of experimental activity has been the demonstration that NSDI phenomenology is applicable to triple and multiple as well as to double ionization and to molecules as well as to atoms. Another development has been an extension to different wavelength regions, most notably substantially longer wavelengths. On the theoretical side, the question of dimensionality has been addressed in a new way by the development of double-ionization theory for elliptically polarized strong fields, with new insights already in focus. Applicability of classical chaos theory is natural to expect any time when strong periodic excitation of a nonlinear system is undertaken, but only recently have results begun to appear that are connected to NSDI. The following sections illustrate all of these, the new frontiers opened by NSDI.

A. Nonsequential double ionization below the recollision threshold intensity

If the maximal return energy of $3.17U_P$ [cf. Eq. (10)] drops below the second ionization potential then the classical recollision model in its simplest (RII) version predicts that the yield of NSDI should immediately vanish. Quantum mechanics does not obey such a sharp cutoff, since it allows, in principle, the electron to absorb an arbitrary number of photons from the field. However, the more photons are absorbed above the classical limit, the less likely such a process becomes. Hence, one still calculates an extremely fast decrease of the yield for low intensity (Kopold *et al.*, 2000). In marked contrast, experimental doubly charged-ion-count data show no such behavior at all and, indeed, the complete absence of any such threshold intensity afforded early arguments against the validity of the recollision model. We see that now this is rather interpreted as an indication of the presence of pathways other than the simplest RII.

COLTRIMS data for the doubly charged-ion momentum and the *e*-*e* correlation also did not exhibit any qualitative change when the laser intensity was reduced below the RII threshold (Eremina *et al.*, 2003; Weckenbrock *et al.*, 2004). These data could be explained by taking into account that the bound electron actually only has to overcome the second ionization potential lowered by the energy of the saddle of the combined potentials of the ion and the laser field (cf. Fig. 2): $I_{P2}^{*} = I_{P2} - 2\sqrt{2|E(t)|}$, where $E(t)$ denotes the laser field at the time of escape (van der Hart and Burnett, 2000).

More recent experiments (Liu *et al.*, 2008, 2010) were carried out at intensities below this limit and even so low that the classical energy of the returning electron is below that of the lowest excited state. At such intensities a qualitative change was observed: for argon, the correlation of the outgoing-electron momenta (their propensity to leaving side by side) changed into an anticorrelation (leaving back to back). This is shown in Fig. 20(a) by the momentum distribution of argon being concentrated in the second and fourth quadrants. An explanation of the mechanism responsible for the anticorrelation was given in the TC framework, which was augmented to allow for tunneling of the second (bound) electron, as a combination of RESI and direct multiple rescattering (Liu *et al.*, 2010; Ye and Liu, 2010). Multiple recollisions, made possible by the presence of the Coulomb potential, are crucial in the latter. No such anticorrelation was observed for neon; the characteristic differences between argon and neon [cf. Figs. 20(a) and 20(c)] were attributed to the low-lying excited states of Ar^{+} and its large electron-impact cross section. Anticorrelation below the RII threshold was also found in TDNE calculations (Haan *et al.*, 2008, 2010).

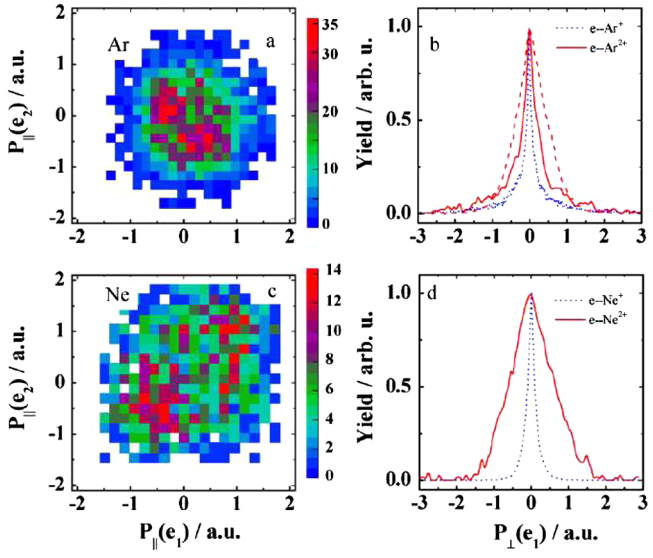

FIG. 20 (color online). Parallel-momentum correlation of the two electrons emitted in NSDI of argon (a) (3×10^{13} W/cm^2) and neon (c) (1.5×10^{14} W/cm^2). (b) Transverse-momentum distributions in coincidence with Ar^{1+} (dotted line) and Ar^{2+} at 3×10^{13} W/cm^2 (solid line) and 7×10^{13} W/cm^2 (dashed solid line) as well as (d) for Ne^{1+} and Ne^{2+} at 1.5×10^{14} W/cm^2. From Liu *et al.* , 2010.

There are still many unresolved issues, especially for neon and in the distribution of the transverse momenta [Figs. 20(b) and 20(d)], which is much wider in the data than in the TC simulation (Liu *et al.*, 2010). Generally, the longitudinal momenta exhibit larger (field-dominated and largely classical) effects and, therefore, have received more attention, but it is the transverse momenta that are expected to reveal imprints of the quantum mechanics involved, since their distribution is determined by the width of the tunneling exit via the uncertainty relation. A comprehensive quantum-mechanical treatment is still lacking (Bondar, Liu, and Ivanov, 2009; Bondar *et al.*, 2011).

B. Other wavelengths producing NSDI

Our current understanding of NSDI is mainly based on the experimental data collected with Ti:sapphire lasers at a center wavelength close to 800 nm. There are several motives that promote studies within a wider wavelength regime.

First, since $U_P \propto I\lambda^2$, long wavelengths allow one to increase the ponderomotive energy at constant intensity. Wavelength, as opposed to intensity, offers a more effective experimental knob to tune the ionization regime into the tunneling regime, which is realized when the Keldysh parameter (7) is small compared with unity. At shorter wavelengths, the intensity required will quickly lead into single-ionization saturation. Longer wavelengths therefore enable one to study a broader category of atomic or molecular targets, which usually possess lower saturation intensities as compared with noble-gas atoms. Also, novel experimental features, characteristic of the long-wavelength NSDI and NSMI dynamics, may be envisioned. Indeed, recent experimental studies of the single-ionization electron spectrum of noble-gas atoms with midinfrared laser pulses have already uncovered qualitatively new aspects (Blaga *et al.*, 2009; Quan *et al.*, 2009), which are under intense discussion.

Second, resonances are strongly wavelength dependent and signal the presence of discrete bound states. Despite the frequent reference to occupancy of excited bound states by the second electron as an intermediate stage toward ionization (e.g., the RESI pathway), there has been little *ab initio* examination of bound-state involvement under NSDI conditions. However, an early step in the direction of understanding bound-state involvement was taken via the TDSE solution by Panfili and Liu (2003). In wavelength scans they found clear resonance effects, i.e., the NSDI engagement of specific bound states (Panfili *et al.*, 2000; Panfili and Liu, 2003). To do this they calculated two-electron wave functions in the 1D AEA approximation, for a model atom whose bound states were accurately calculated. A range of laser wavelengths (in the neighborhood of frequency-doubled 800 nm pulses) was explored and NSDI knee enhancements were clearly associated with bound-state resonances. A different approach to wavelength dependence was taken by Chen, Kim, and Nam (2003), by means of a TC calculation of the double-to-single ionization ratio for a model neon atom. They found that the ratio falls nearly monotonically over a wide range, from 250 to more than 1000 nm.

Experimentally, for short wavelengths no knee was observed for double ionization of helium at 248 nm (Kondo *et al.*, 1993). So far, only very few experimental attempts have been made to explore the NSDI and NSMI dynamics at long wavelengths, which were confined to ion-yield and ion-momentum measurements. For NSDI of xenon, Kaminski *et al.* (2006) found a pronounced wavelength dependence, implying that a resonance mechanism, normally neglected in the studies at the single wavelength of 800 nm, may play a role. Gingras, Tripathi, and Witzel (2009) extended this investigation to an almost continuous scan of wavelengths between 500 and 2300 nm over 2 orders of magnitude in intensity. The differential ion-momentum distributions in NSDI of argon and neon at wavelengths up to 2000 and 1300 nm have recently been measured, respectively, by Alnaser *et al.* (2008) and by Herrwerth *et al.* (2008). The longer wavelength made it possible to explore NSDI of argon deep into the recollision regime and, indeed, the imprints of recollision and impact ionization were distinctly observed (cf. Sec. V.E). Many more detailed studies, e.g., kinematically complete measurements with the COLTRIMS technique, are expected to appear in the near future, advancing a comprehensive understanding of the NSDI and NSMI dynamics over a larger range of wavelengths.

C. Strong-field ionization with elliptical polarization

Almost all NSDI experiments have been carried out with linearly polarized laser pulses. The recollision model, as usually understood, naturally argues against successful NSDI with any substantial amount of ellipticity, because electronic orbits that start at the position of the ion with zero velocity experience a sideward push so that they are not able to revisit the ion. Early experiments (Fittinghoff *et al.*, 1992; Dietrich *et al.*, 1994) confirmed that NSDI production drops rapidly as a function of ellipticity ε and was not detectable beyond $\varepsilon \approx 0.25$. This was supported by

an early TDNE calculation with circular polarization for helium by Lerner, LaGattuta, and Cohen (1996) and interpreted as strong support for the recollision model. However, in clear conflict with the recollision scenario, several later observations of NSDI were reported under circular polarization (Gillen, Walker, and Van Woerkom, 2001; Guo and Gibson, 2001). These observations have not been fully explained to date, and development of the theory of high-field double ionization with other than linear polarization has begun only recently.

Observable consequences of high-field elliptical polarization have begun to be reported in the SDI regime (Maharjan *et al.*, 2005; Pfeiffer, Cirelli, Smolarski, Dörner, and Keller, 2011), and also in large-molecule fragmentation and ionization (Hertel *et al.*, 2009).

For elliptical polarization the SFA approach has been explored by Shvetsov-Shilovski *et al.* (2008), the TC approach by Hao *et al.* (2009), and the TDNE approach by Wang and Eberly (2009a, 2009b, 2010a, 2010b). An elliptically polarized field has major and minor axes, which we take to be in the x and y directions, respectively, and write as follows, for ellipticity ε:

$$\mathbf{E}(t) = E_0 f(t)[\hat{\mathbf{x}}\sin(\omega t + \phi) + \hat{\mathbf{y}}\varepsilon\cos(\omega t + \phi)], \quad (26)$$

where $f(t)$ is the field's smooth several-cycle envelope function. The simpleman view of this elliptically polarized case gives the velocities along the x and y directions as (having put $f = 1$)

$$v_x(t) = \frac{1}{\omega}E_0[\cos(\omega t + \phi) - \cos(\omega t_0 + \phi)], \quad (27)$$

$$v_y(t) = v_{0y} - \frac{\varepsilon}{\omega}E_0[\sin(\omega t + \phi) - \sin(\omega t_0 + \phi)]. \quad (28)$$

Although the elementary theory of tunnel ionization has zero longitudinal electron velocity, $v_{0x} = 0$ at t_0, the moment of tunneling release, there is a significant transverse velocity distribution whose width, by the uncertainty relation, is associated with the width of the tunnel exit; see, e.g., Delone and Krainov (1998) and the discussion in Sec. IV.D. A distribution of values of this transverse component allows completely elliptical returns to the nucleus for every ellipticity value (Kopold, Milošević, and Becker, 2000). Two examples of such trajectories taken from TDNE calculations are shown in Fig. 21. One possible consequence is an explanation for the circular polarization NSDI data mentioned above (Wang and Eberly, 2010a).

If compensation and recollision do not occur, but the intensity is sufficient, the second electron may still be ionized in an independent SDI event. This type of SDI also has an elliptical signature (Wang and Eberly, 2009a, 2009b) and it is easy to describe. When at $t = t_0$ the major-axis field first satisfies the over-barrier value we can take $\sin(\omega t_0 + \phi) \approx \pm 1$, and drop the cosine term $\cos(\omega t_0 + \phi)$ in Eq. (27). Thus $v_x(t)$ is purely oscillatory and v_{0y} contains all of the drift velocity away from the ion, so momentum is transferred through recoil to the ion only along the minor axis. The effect is known for single ionization (Goreslavski *et al.*, 1996) and has been dubbed the "dodging" effect: the electron dodges

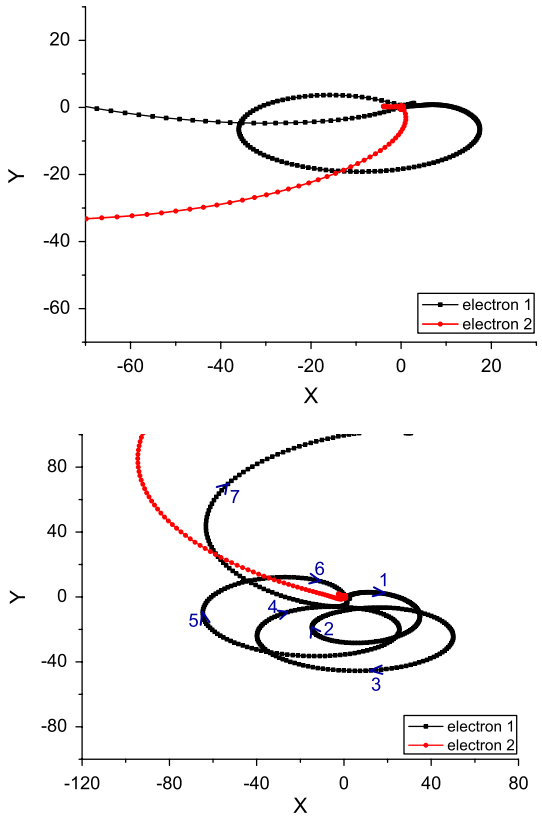

FIG. 21 (color online). Recollision events under elliptical polarization. Top: A nearly perfectly elliptical trajectory by one electron makes a recollision in the first postionization cycle, and both electrons are freed. Bottom: A sequence of near-elliptical circulations is pulled by nuclear attraction into a double-ionizing recollision after several near misses. From Wang and Eberly, 2010b.

the major component of the elliptically polarized field (Paulus *et al.*, 1998).

For double ionization, this is a new observable aspect originating in nonzero ellipticity. Because of the $\pm$ dichotomy arising from phase ambiguity there will be two transverse recoil peaks predicted for the first electron, four peaks for the first two electrons (the SDI case), and 2^n peaks for n-electron ionization, if accessible. Exactly the four peaks for double ionization were seen in TDNE calculations (Wang and Eberly, 2009b), and subsequently found in SDI momentum data (see Fig. 22) reported by Maharjan *et al.* (2005) and later by Pfeiffer, Cirelli, Smolarski, Dörner, and Keller (2011).

A related feature of elliptical polarization appears to prove useful in pursuing the possible breakdown of the SAE approximation. For values of E_0 too high to be compensated by any available initial v_{0y} value, recollisions can be avoided with certainty. This opens to view the effects of so-called "precollisions," i.e., the energy exchanges between the two electrons before either one is ionized. Many such precollision events are easily seen in both TDNE and phase-space simulations, as shown in Figs. 7 and 19.

The unexpected and highly anomalous effect of this is an SDI knee in the ion-count data, i.e., a knee in the absence of any recollisions (Wang and Eberly, 2011). The knee can be interpreted as a consequence of the precollisions. A series of recent SDI observations (Pfeiffer, Cirelli, Smolarski, Dörner,

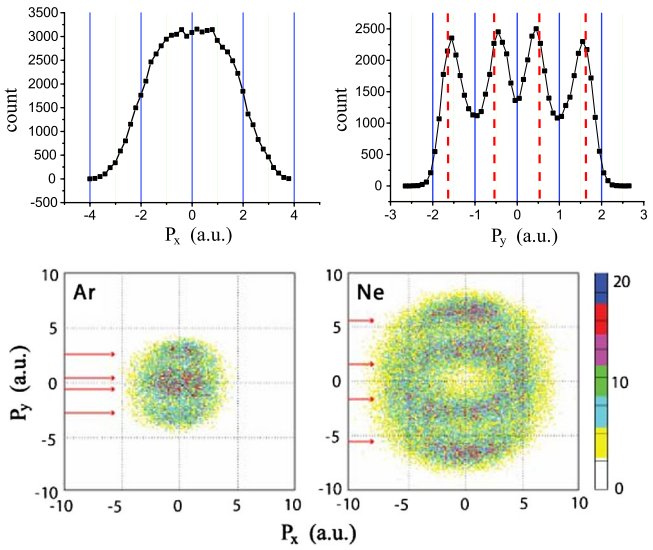

FIG. 22 (color online). Top panels: Predicted longitudinal and transverse ion-momentum distributions from Wang and Eberly (2009b) for $\varepsilon = 0.5$. Bottom panels: Experimental results from Maharjan *et al.* (2005) for Ne and Ar atoms and $\varepsilon \sim 0.8$. The experimental distributions have only a single broad peak along the P_x axis, consistent with the theoretical curve in the top left panel. The arrows indicate four transverse P_y peak positions of the type predicted in the top right panel.

and Keller, 2011; Pfeiffer, Cirelli, Smolarski, Wang *et al.*, 2011) on neon and argon, challenging the SAE with elliptically polarized irradiation, are consistent with this TDNE modeling. A challenge to the SAE approximation in the high-field domain has not previously been feasible and would be important to all of the step-by-step theoretical approaches, with implications for Keldysh's near-optical static tunneling theory.

D. Phase-space perspective and classical chaos

Periodically driven nonlinear systems of high enough dimension are always susceptible to classically chaotic evolution if the driving force is strong enough; see, for example, the discussion by Milonni, Shih, and Ackerhalt (1987). Studies of quantum chaos have been well known for decades, using microwave ionization of Rydberg atoms as the experimental test bed; see, for example, first reports by Bayfield and Koch (1974) and early analyses by Leopold and Percival (1978, 1979). Two-electron NSDI is certainly an example of a multidimensional physical system excited periodically, and the laser excitation is obviously very strong, so chaotic dynamics should be evident.

Surprisingly, the analytical techniques familiar in classical chaos theory have only recently begun to be applied to NSDI by the Uzer group (Mauger, Chandre, and Uzer, 2009, 2010a). So far, results are based on calculations for an artificial atom with two electrons built from the Rochester soft-core potentials (16) using the AEA mentioned in the Introduction. A principal result is a new interpretation of the famous knee shape, which the classical phase-space calculations nicely reproduce (see Fig. 10). It is ascribed (Mauger, Chandre, and Uzer, 2010a) to a superposition of a monotonic rapid increase in ion counts versus I at high intensities with a bell-shaped distribution of ion counts at lower intensities, between the intensities that are too low for ionization and those that are too high for effective recollision where sequential ionization takes over.

Results from the phase-space analysis can, in principle, be compared with those obtained via both TDSE solutions (Panfili, Eberly, and Haan, 2001; Haan *et al.*, 2002) and classical ensemble calculations (Panfili, Haan, and Eberly, 2002) for the same atom under the same laser pulse. An example of this appears in Mauger, Chandre, and Uzer (2009). The two electrons are identified with distinct "inner" and "outer" labels during their bound evolution, but quick switches of label occur between them. This is exactly what one sees prior to ionization in classical two-electron energy versus time plots such as Figs. 7 and 18.

The phase-space approach is also able to analyze circular polarization by employing a rotating frame transformation, and the results are striking. Mauger, Chandre, and Uzer (2010b) report calculations showing that an NSDI knee is predicted for a model magnesium atom, but not for the corresponding model helium atom. Under circular polarization the knee's absence in helium conforms to both experimental data and the early TDNE result of Lerner, LaGattuta, and Cohen (1996), but the contrary prediction of the knee's presence for magnesium is the first theoretical report in agreement with the long-standing data of Gillen, Walker, and Van Woerkom (2001).

Given the long-known effectiveness of chaos-dominated analyses of microwave ionization of single electrons in Coulombic potentials, it is very likely that similarly productive insights may come from further work on NSDI from the standpoint of a phase-space perspective.

E. NSDI of molecules

Soon after the discovery of the pronounced knee structure in the double-ionization yield of helium as a function of laser intensity, experiments revealed that this knee structure, the footprint of a nonsequential channel, also appears in double ionization of small molecules (Talebpour, Larochelle, and Chin, 1997; Cornaggia and Hering, 1998, 2000). The first evidence that electron recollision is also responsible for nonsequential double ionization of the simplest molecule, molecular hydrogen, came from the ellipticity dependence of the yields of the charged ionic fragments, emitted after molecular double ionization (Niikura *et al.*, 2002; Alnaser *et al.*, 2003). This was confirmed later by differential COLTRIMS measurements, which found that the correlated electron-momentum distribution in NSDI of diatomic molecules (e.g., N_2) peaks at nonzero parallel momenta (Eremina *et al.*, 2004; Zeidler *et al.*, 2005). These findings provide solid evidence that electron recollision plays a major role in molecular NSDI.

Novel aspects of the NSDI dynamics of molecules are related to the structural complexity and the extra nuclear degrees of freedom of molecular systems. For example, the correlated electron-momentum distribution in NSDI of

diatomic molecules exhibits strong dependence on the ground-state orbital symmetries (Eremina *et al.*, 2004) and on the alignment of the internuclear axis with respect to the laser polarization axis (Zeidler *et al.*, 2005).

These NSDI features pose a challenge to theory. A full-dimensional TDSE solution is out of the question for this more-than-three-body problem. An advance via the TC approach (Liu *et al.*, 2007) succeeded in reproducing the experimental results, especially the knee, for NSDI of N_2 (Cornaggia and Hering, 2000). However, TC theories and TDNE theories as well will be confronted with the following problem: The multicenter nature of molecules is likely to lead to structural interference effects. Structural symmetries are classical effects, but quantum interferences arising from them are not. Such structural interference has been shown to play a significant role in the closely related one-electron strong-field phenomena induced by electron recollision, such as HHG of molecules (Lein *et al.*, 2002) and ATI of molecules (Muth-Böhm, Becker, and Faisal, 2000; Okunishi *et al.*, 2009; Kang *et al.*, 2010). The FD method, being an intrinsically quantum-mechanical model, can in principle account for this interference effect and has been recently employed to address the dependence of NSDI on molecular structure and alignment (Figueira de Morisson Faria *et al.*, 2008, 2009; Jia *et al.*, 2008, 2009). Nevertheless, owing to its complexity, more theoretical efforts are required to achieve a deeper understanding of NSDI of molecules.

F. NSDI with few-cycle pulses

The essential NSDI dynamics in the context of the rescattering scenario unfold within one optical cycle. Simple as it may appear, its comprehensive verification is still frustrated by the experimental fact that usually the effects of many field cycles are superimposed. It is therefore desirable to apply a laser pulse that is so short that it allows only one reencounter of the first-ionized electron with its parent ion. Such a few-cycle pulse, in addition to its duration, carrier frequency, amplitude, and polarization, depends on one more parameter, the carrier-envelope (CE) phase ϕ, which specifies the phase offset between the maximum of the envelope and the nearest maximum of the carrier wave. The field then can be written in the form $E(t) = E_0 f(t) \sin(\omega t + \phi)$, where the envelope $f(t)$ is assumed to be maximal at $t = 0$ (Brabec and Krausz, 2000). Then, for a very short pulse, different values of ϕ give rise to different electric-field forms with, correspondingly, different manifestations in physical processes induced by the pulse, for example, in the above-threshold ionization spectra (Paulus *et al.*, 2001); for a review, see Milošević *et al.* (2006).

The first experimental attempt along this direction was performed by Liu *et al.* (2004). They employed a few-cycle laser pulse with a duration of 5 fs at a center wavelength of 760 nm and measured the momentum distribution of the doubly charged Ar^{2+} ion. The experiment showed that the ion-momentum distribution reacts sensitively to the CE phase. It also showed a strongly suppressed contribution of the RESI channel, indicated by a more pronounced dip at zero momentum.

More information about the NSDI dynamics is revealed by a study of the electron-electron momentum correlation with a laser pulse approaching the single-cycle limit. Theoretically this was addressed by Liu and Figueira de Morisson Faria (2004) within the classical analog (21) of the quantum-mechanical S-matrix treatment of NSDI, by Xin, Ye, and Liu (2010) with the TC method, and by Shaaran, Figueira de Morisson Faria, and Schomerus (2011) with fully quantum-mechanical S-matrix simulations. Simulations for NSDI by a polarization-gated pulse, represented by two counterpropagating circularly polarized phase-stabilized few-cycle pulses with a finite delay, were carried out by Quan, Liu, and Figueira de Morisson Faria (2009), using the classical analog (21) of the quantum-mechanical S-matrix formulation. Pertinent experiments will be made possible by a new technique, which eliminates the need to stabilize the CE phase throughout the experimental runs. As proposed by Johnson *et al.* (2011), the CE phase of few-cycle laser pulses operating in a nonstabilized mode can be tagged on a shot-by-shot basis. The results can be sorted and coordinated later using the phase-value tags. Such experiments are underway on Ar^{2+} by Bergues *et al.* Observation of a characteristic cross shape with its center at zero momenta in the CE-phase-averaged momentum-momentum correlation (Shaaran, Figueira de Morisson Faria, and Schomerus, 2011) would add important weight to the RESI route as the dominant pathway for NSDI of argon. Further electron-electron correlation spectra, recorded with COLTRIMS for few-cycle pulses at specified CE phase, will certainly be available soon and provide the most detailed information yet about the NSDI dynamics.

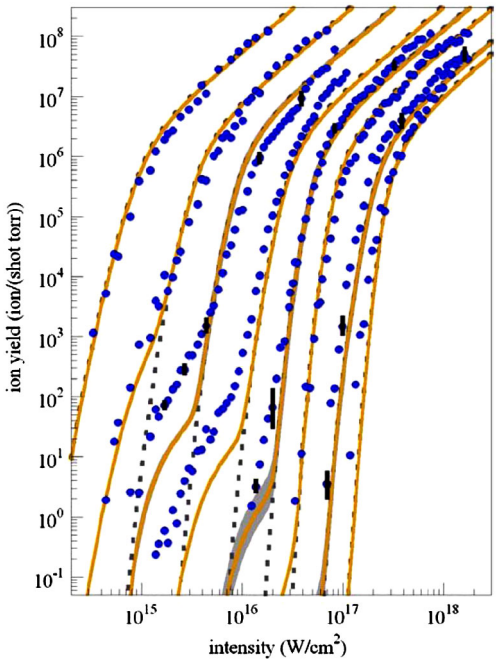

FIG. 23 (color online). Experimental (circles) Ne^+ to Ne^{8+} (left to right) yields and the corresponding ADK yields (dashed lines) as well as a calculation including the relativistic drift (solid lines). Knee signatures are clearly visible for Ne^{2+} to Ne^{5+}. From Palaniyappan *et al.*, 2005.

G. Nonsequential multiple ionization

In total ion-yield measurements of high-field multiple ionization ($N \geq 3$), a significant contribution of one or several nonsequential channels has frequently been identified (Augst *et al.*, 1995; Larochelle, Talebpour, and Chin, 1998; Maeda *et al.*, 2000; Palaniyappan *et al.*, 2005, 2006); see Fig. 23 for an example.

The full description of NSMI processes poses an obvious challenge to theory. There is no currently realistic prospect for extending the full TDSE treatment of irradiation at laser wavelengths around 800 nm to include the electron-electron interactions between more than one pair of electrons. At much higher photon energy, for $\hbar\omega \approx 80$ eV, Ruiz, Plaja, and Roso (2005) calculated the time dependences of single, double, and triple ionization of lithium by solving the TDSE in the AEA limit, and briefly explored the role of wave function symmetry, an issue in need of extended attention in high-field multielectron contexts.

In the basic case of ion-count data, N-fold rate equations can be used (Becker and Faisal, 1999b) for systematic calculation. These must include all N ionic charge states and all sequences of single and nonsequential multiple ionization processes. The results reproduce the ion-count data in xenon (up to Xe^{6+}) very well. Note that the ADK rates (Ammosov, Delone, and Kraĭnov, 1986) strongly depend on the magnetic quantum number m, so different m channels must be distinguished in the rate equations. This also raises the question of how fast relaxation between different m states occurs (Taïeb, Véniard, and Maquet, 2001). For krypton, it appears to be sufficiently fast to erase any transient core polarization (Gubbini *et al.*, 2005a).

High charge states require for their production fields in excess of some 10^{16} W/cm^2. For such fields, the Lorentz force $\mathbf{v} \times \mathbf{B}$ can no longer be ignored. The resultant $\mathbf{E} \times \mathbf{B}$ drift more and more prevents the electron from recolliding with its parent ion and begins to invalidate the dominance of the recollision mechanism. Indeed, the highest charge states of xenon observed at 1.57×10^{18} W/cm^2 (Xe^{19+} to Xe^{21+}) showed no evidence of a nonsequential contribution (Dammasch *et al.*, 2001). Absence of nonsequential ionization was also observed for the highest charge states (7+ and 8+) in neon starting at 10^{17} W/cm^2 (Palaniyappan *et al.*, 2005); cf. Fig. 23, and for krypton (up to 11+) between 10^{17} and 10^{18} W/cm^2 (Gubbini *et al.*, 2005b).

Differential measurements become necessary in order to achieve more physical insight, and with the help of the COLTRIMS technique, first steps have been made in the study of nonsequential triple and quadruple ionization (NSTI and NSQI) of neon and argon (Moshammer *et al.*, 2000; Rudenko *et al.*, 2004; Zrost *et al.*, 2006). In neon, a well-pronounced double-hump structure, the trademark of the RII mechanism, was observed in the ion-momentum distribution along the laser polarization. In contrast, for argon a considerable fraction of ions with small momenta was found. This difference between neon and argon, which bears much similarity with NSDI data, has been explained as due to the additional contribution of the RESI mechanism. These differential ion-momentum measurements provided evidence that the physical mechanism behind NSMI (at least up to quadruple ionization) is to a great extent similar to its NSDI counterpart.

In the S-matrix framework, the single Feynman diagram, which considers only the simplest RII pathway (as shown in Fig. 9), will be replaced by a large number of more complicated diagrams. Hence, any straightforward extension of the FD approach appears to be all but impossible. At present, this leaves two routes for theoretical attack on NSMI, as follows.

The first route is the extension of both TDNE and TC models to NSMI. This is conceptually simple and feasible, but requires a large expansion of the trajectory ensemble and thus significant computational resources. Nevertheless, the TDNE method has been pursued up to fourfold ionization (Ho, 2007), and employed to calculate three-electron trajectories in NSTI (Ho and Eberly, 2006), although in a reduced 2D fashion. The knee structure in the ion yield was reproduced, and back-analysis of the triply ionizing trajectories provided straightforward evidence that the recollision mechanism plays a major role in NSTI.

Figure 24 presents a comparison of TDNE model calculations and experimental data for double and triple ionization of argon. The agreement is surprisingly good. At an intensity of 0.8 PW/cm^2, single ionization is saturated and double ionization proceeds sequentially. Hence, the doubly charged ion-momentum distribution is rather narrow with a maximum at zero momentum. However, the triply charged ion momentum exhibits a double hump, indicating that it is caused by a nonsequential process. Indeed, an NSDI process can start from the singly charged ion. The maximum of the ion-momentum distribution occurs at about $2\sqrt{U_P}$ in both the data and the TDNE simulation. This is much below the simpleman estimate of $6\sqrt{U_P}$ for the $Ar \rightarrow Ar^{3+}$ nonsequential channel, which rather seems to act as a cutoff. It is also below the $4\sqrt{U_P}$ simpleman estimate for the sequential–nonsequential $Ar \rightarrow Ar^{+} \rightarrow Ar^{3+}$ process, where the nonsequential process starts from the singly charged ion. Further efforts to extract the differential ion and electron-momentum distributions and to compare them with the available data can be expected.

The second route follows a straightforward generalization of the classical-kinematics model (21) from NSDI to multiple nonsequential ionization. Two modifications are implemented: First, the available energy now is $E_{\mathrm{ret}}(t) - I_P(N)$, where $I_P(N) = \sum_{n=2}^{N} I_{Pn}$ denotes the sum of the second to the Nth ionization potential. Second, the process of distributing this energy over the final N free electrons is allowed to take

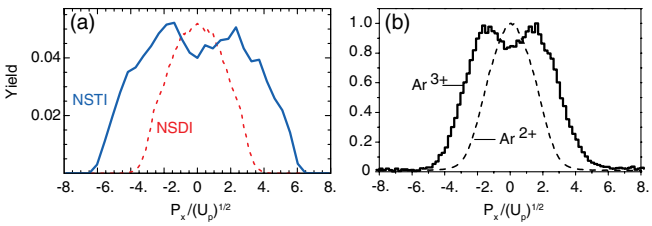

FIG. 24 (color online). Two-electron and three-electron longitudinal ion-momentum distributions for double (DI) and triple (TI) ionization of argon by 780 nm laser pulses at 0.8 PW/cm^2. The left-hand panel shows the results of TDNE calculations, the right-hand panel the data of Zrost *et al.* (2006). From Ho and Eberly, 2007.

some time Δt (Liu *et al.*, 2006; Liu, Figueira de Morisson Faria, and Becker, 2008), which is referred to as a thermalization time. The N-electron distribution is then given by

$$F(\mathbf{p}_1, \ldots, \mathbf{p}_N) = \int dt_0 w(t_0) \delta\Big(\frac{1}{2}\sum_{i=1}^{N}[\mathbf{p}_i + \mathbf{A}(t+\Delta t)]^2 + I_P(N) - E_{\mathrm{ret}}(t)\Big). \quad (29)$$

The form factor $|V_{\mathbf{p}-\mathbf{k}}|^2$, which contained the dynamics of the electron-electron interaction in Eq. (21), has just been dropped. The distribution (29) provides the simplest description of NSMI conceivable as it relies on nothing but energy conservation and the recollision kinematics. All of the complicated dynamics of the process has been lumped into the thermalization time Δt.

With the recollision occurring at time t, the delay Δt determines the time $t + \Delta t$ at which the N electrons will be set free. Since the recollision takes place approximately at a zero crossing of the laser field [when $\mathbf{A}(t)$ is maximal], a value of $\Delta t \approx T/4$ will delay the release of the electrons until the next extremum of the field [when $\mathbf{A}(t+\Delta t) \approx 0$] when the subsequent acceleration of the released electron is near zero. This can be seen in Fig. 25, which compares the data of Zrost *et al.* (2006) for NSQI of argon with results from the statistical model (29) with no delay ($\Delta t = 0$) and with a delay of about a quarter cycle ($\Delta t = 0.265T$), which was chosen to yield an optimal fit. For $\Delta t \approx T/4$ the model condensed in Eq. (25) has much in common with the RESI scenario discussed above, except that here all N electrons are delayed, while for RESI it is $N-1$; the returning electron scatters without the delay. However, the model (29) was also modified (Liu, Figueira de Morisson Faria, and Becker, 2008) to simulate the latter case, referred to as a "glancing recollision." For $N > 2$, the differences between such glancing recollisions and the standard "hard recollision" were found to be not very pronounced. Regarding Fig. 25 we conclude that while the distribution obtained in the absence of a delay shows no similarity with the data, the one with the best-fit delay displays excellent agreement. This suggests that the simple assumption of a delay (modeling the concept of thermalization) sometimes can parametrize and capture the complicated dynamics quite well.

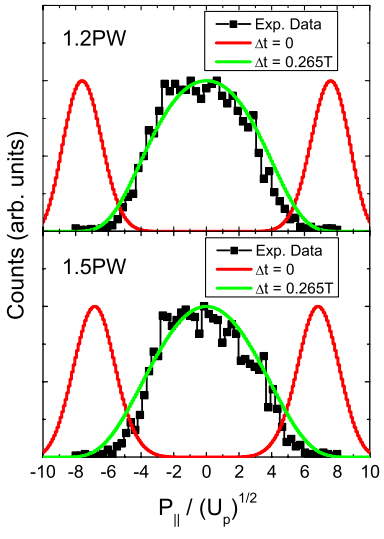

FIG. 25 (color online). Distribution of the longitudinal ion momentum for NSQI of argon at 1.2 PW/cm^2 (upper panel) and 1.5 PW/cm^2 (lower panel). The curves (squares) are the experimental data from Fig. 1 of Zrost *et al.* (2006). The remaining curves are calculated from Eq. (29) for $\Delta t = 0$ and $\Delta t = 0.265$. From Liu, Figueira de Morisson Faria, and Becker, 2008.

The argument for a thermalization process obtains some support from a TDNE report (Ho and Eberly, 2006), which displays in snapshot fashion a three-way energy sharing event during a recollision. This can be interpreted as a thermalization process, although only 20–30 attoseconds in duration. Time delays between rescattering and double ionization were also observed and commented in TDNE simulations by Ho and Eberly (2005) and Haan *et al.* (2006). The distribution (29) can also be seen as an attempt to make a virtue out of necessity since accounting for the various electron-electron and electron-ion interactions is a hopeless task for quantum theory. The result then is a statistical model of the type that has been employed before in similar cases in molecular or high-energy physics when the underlying dynamics were unknown or just too complicated [see, e.g., Hagedorn (1965) and Forst (1973)].

The $3e$ TDNE calculations (Ho and Eberly, 2006, 2007) deserve mention on another ground as well. They were the first and possibly still are the only calculations with more than two electrons that are simultaneously fully active. In this respect they go beyond other existing calculations to corroborate the integrity of the recollision picture. They do this by confirming that the double-ionization features (knee, etc.) are still reproduced even when more than two electrons are allowed to participate.

VII. SYNOPSIS AND OUTLOOK

In summary, we reviewed the unusual situation existing in atomic physics in which four approaches to multiphoton double-ionization theory are conceptually as well as calculationally distinct and, at the same time, successful. All have been productive in increasing understanding of the new phenomena uncovered by short-pulse high-field optical or near-infrared irradiation of atoms and molecules. We first identified them within two categories, the all-at-once category including the TDSE and the TDNE approaches, and the step-by-step category including the FD and the TC approaches.

Figure 10 displays the evidence that both categories are represented by theories capable of reproducing the key experimental signature of nonsequential double ionization, which is the presence of a prominent knee in an ion-count versus intensity plot. However, it has been made clear that none of the four approaches is perfect or even complete. The physical reason is the congruence of several nearly equally strong forces acting on the active atomic electrons, making a challenge too great to be fully overcome by any one of the approaches. It is not hard to summarize the flaws in each approach. This provides one way to assess what can be accomplished with each.

The main flaw in the step-by-step approach is that there are no truly fundamental guides that determine which step to

take, i.e., which physical process to attend to at any given time, nor in what sequence. The practical impossibility of designing a systematically consistent perturbation-based sequence of steps is then overcome by adopting a certain scenario for how an NSDI event takes place. Especially, two such scenarios have been considered, which are shown in Feynman-diagram form in Fig. 9. For the rescattering with the RII scenario, one asserts that the first electron is released at an unknown time by tunneling, and that subsequently the second is ejected by collision with the first. We showed that substantial agreements with experimental facts are achieved when the step-by-step approach is guided by these two assertions. Other scenarios may also contribute or even be dominant in some situations, such as the RESI scenario for some atoms and/or below the threshold for rescattering-impact ionization. In some cases, agreement is improved if the nature of the electron-electron collisional force is modeled with a contact potential rather than the fundamental Coulomb form. As explained, this can be taken as a way to account for the otherwise unmentioned behavior of core electrons.

The weak point in the all-at-once approach is its near impossibility of execution. However, it has been implemented many times, similar to the step-by-step approach, by reliance on assertions that have not been fundamentally justified. These assertions have a degree of intuitive rationale. Their basis is one or more of several simplifications that stop short of solving the two-electron TDSE in all details. One simplification has been to reduce the dimensionality of the space in which the electrons are allowed to move. This is the AEA, based on the intuitive notion that the electrons' motion will be closely aligned with the laser polarization, usually linear.

A different simplification has been to replace the Schrödinger equation with the analogous time-dependent Newton equation and apply it to a large microcanonically random ensemble of pairs of electrons. This appears outrageously wrong headed at first, but has shown unexpected value in matching key features of experimental data. It is based on the hint provided in Fig. 4, which displays a mid-pulse snapshot of one-dimensional calculations that show strong similarity of two spatial probability distributions obtained from a quantum TDSE wave function and a TDNE ensemble of classical electron pairs, under identical conditions of wavelength, intensity, pulse shape, etc. One exception to these simplifications is the solution of the TDSE for two electrons in full dimensionality in the case of helium. Here the weak point is that results are fully available only for wavelengths shorter than the regime where most NSDI data exist and, in all likelihood, will remain restricted to the case of helium.

Interestingly, both all-at-once and step-by-step approaches have quantum and classical variants. Also, one should say that the two approaches are cooperative as much as competitive. For example, the classical all-at-once TDNE approach uses only classical electrons moving on definite trajectories starting from a random microcanonical distribution of positions and momenta. There is no built-in assumption about a possible later collision of one electron with the other. Nevertheless, examination of its successful NSDI trajectories shows that under high-field laser forces recollision is exactly what happens. Thus its successes validate the main assertion of the step-by-step approach. Similarly, the variability among the best choices for electron-electron scattering potential in implementing FD calculations can be seen as support for choices made for the soft core of the potentials adopted for the TDNE equations.

On the very positive side, each of the approaches has strong points that deserve to be highlighted. The all-at-once approaches of TDSE and TDNE are unique in allowing all terms in the two-electron Hamiltonian to participate without interruption throughout the NSDI process, from the time the laser field starts with zero strength until it turns off. The TDSE results of the Taylor group are alone in achieving striking matches to experimental data without mathematical compromises. There is no other approach that can claim this, even if it applies only to data from helium and wavelengths shorter than those of main interest. The TDNE approaches, carried out in detail by the Haan and Eberly groups, emphasized the interpretive value of classical two-electron trajectories en route to NSDI. The TDNE approaches are so flexible that they have successfully entered all experimental NSDI domains of wavelength and intensity and have been able to provide results for topics such as elliptical polarization and triple and quadruple ionization in advance of detailed experiments.

The step-by-step approaches also have significant success to their credit, such as the quantitative reproduction within the quantum-mechanical FD approach of the knees for a variety of atoms and laser parameters or of the electron momentum-momentum correlation for neon. The TC approach produced good agreement with experimental data since its inception. As a recent success, we mention the calculation of the finger-like structure in the electron momentum-momentum correlation in helium, shown in Fig. 14.

The greatest strength of the FD approach may be the proper description of genuine quantum features, such as interference and tunneling. Analysis of the results of the FD approach has not identified any distinct footprints of tunneling (Ho, Liu, and Becker, 2007), but very pronounced interference effects are predicted by FD theory. They are most visible in fully differential results where ideally all electron-momentum components are observed. Because of poor statistics, such data are not yet available. Focal averaging also tends to smear out the imprints of interference. However, two-center structural interference effects may become accessible in aligned molecules in the near future.

Given the practical and conceptual limitations of the all-at-once and the step-by-step avenues, a combined route may turn out to be most efficient for the foreseeable future when it comes to simulating particular experimental results: the TC approach, which combines step-by-step and all-at-once features, will serve well whenever the atomic state initiating a true tunneling event must be specified. The subsequent TC dynamics are described classically all at once by the TDNE procedure. The TC approach allows one to introduce atom-specific parameters, such as individual first and second ionization potentials. As it stands, the conceptual shortcomings of the TC approach—no quantum interference in the final state and no coherent interplay between tunneling and subsequent evolution—seem to

have little practical significance. Currently, the TC approach appears to be the only one that allows for better-than-qualitative atom-specific results for a broad range of atoms. As one can expect, its few drawbacks arise from those strengths. The assumption of tunneling as an abrupt midpulse event without antecedents is powerfully useful, but when this assumption fails and antecedent events have consequences, only the TDNE and TDSE approaches can be employed, despite their shortcomings already noted.

Besides explaining and describing the rich phenomenology that is exhibited experimentally, the theories of NSDI (and NSMI) draw their interest and significance from the fact that very different theories allow views from very different perspectives but ultimately provide convergent insights. This is possible because the few-particle systems of interest are still within the grasp of all-at-once methods, so that step-by-step models can be tested not only by comparison with physical reality, but also with the much more detailed and controlled reality of all-at-once calculations. A fascinating side effect is the rare chance to assess the quantumness of a few-particle system in an external field.

ACKNOWLEDGMENTS

We have benefited from discussions with P. Agostini, A. Bandrauk, A. Becker, S. L. Chin, J. Chen, P. B. Corkum, R. Dörner, U. Eichmann, C. Figueira de Morisson Faria, S. L. Haan, S. P. Goreslavski, M. Yu. Ivanov, D. B. Milošević, R. Panfili, S. V. Popruzhenko, H. R. Reiss, L. Roso, H. Rottke, A. Saenz, W. Sandner, O. Smirnova, A. Staudte, K. T. Taylor, J. Ullrich, D. Villeneuve, and X. Wang. This work was supported by US DOE Grant No. DE-FG02-05ER15713. P. J. H. acknowledges support from Deutscher Akademischer Austausch Dienst (DAAD) (Grant No. A0514377). X. L. acknowledges support from the NNSF of China (Grant No. 10925420) and the National Basic Research Program of China (Grant No. 2011CB8081002).

REFERENCES

Agostini, P., and L. F. DiMauro, 2008, Contemp. Phys. **49**, 179.
Aleksakhin, I. S., I. P. Zapesochnyi, and V. V. Suran, 1977, JETP Lett. **26**, 11.
Alnaser, A. S., D. Comtois, A. T. Hasan, D. M. Villeneuve, J.-C. Kieffer, and I. V. Litvinyuk, 2008, J. Phys. B **41**, 031001.
Alnaser, A. S., T. Osipov, E. P. Benis, A. Wech, B. Shan, C. L. Cocke, X. M. Tong, and C. D. Lin, 2003, Phys. Rev. Lett. **91**, 163002.
Ammosov, M. V., N. B. Delone, and V. P. Kraĭnov, 1986, Zh. Eksp. Teor. Fiz. **91**, 2008 [Sov. Phys. JETP **64**, 1191 (1986)].
Augst, S., A. Talebpour, S. L. Chin, Y. Beaudoin, and M. Chaker, 1995, Phys. Rev. A **52**, R917.
Bauer, D., 1997, Phys. Rev. A **56**, 3028.
Bauer, D., and F. Ceccherini, 2001, Opt. Express **8**, 377.
Bayfield, J. E., and P. M. Koch, 1974, Phys. Rev. Lett. **33**, 258.
Bebb, H. B., and A. Gold, 1966, Phys. Rev. **143**, 1.
Becker, A., R. Dörner, and R. Moshammer, 2005, J. Phys. B **38**, S753.
Becker, A., and F. H. M. Faisal, 1996, J. Phys. B **29**, L197.
Becker, A., and F. H. M. Faisal, 1999a, Phys. Rev. A **59**, R1742.
Becker, A., and F. H. M. Faisal, 1999b, Phys. Rev. A **59**, R3182.
Becker, A., and F. H. M. Faisal, 2000, Phys. Rev. Lett. **84**, 3546.
Becker, A., and F. H. M. Faisal, 2002, Phys. Rev. Lett. **89**, 193003.
Becker, A., and F. H. M. Faisal, 2005, J. Phys. B **38**, R1.
Becker, W., F. Grasbon, R. Kopold, D. B. Milošević, G. G. Paulus, and H. Walther, 2002, Adv. At. Mol. Opt. Phys. **48**, 35.
Becker, W., A. Lohr, and M. Kleber, 1994, J. Phys. B **27**, L325 J. Phys. B **28**, 1931 (1995) (corrigendum).
Becker, W., and H. Rottke, 2008, Contemp. Phys. **49**, 199.
Bhardwaj, V. R., S. A. Aseyev, M. Mehendale, G. L. Yudin, D. M. Villeneuve, D. M. Rayner, M. Yu. Ivanov, and P. B. Corkum, 2001, Phys. Rev. Lett. **86**, 3522.
Blaga, C. I., F. Catoire, P. Colosimo, G. G. Paulus, H. G. Muller, P. Agostini, and L. F. DiMauro, 2009, Nature Phys. **5**, 335.
Bondar, D. I., W.-K. Liu, and M. Yu. Ivanov, 2009, Phys. Rev. A **79**, 023417.
Bondar, D. I., G. L. Yudin, W.-K. Liu, M. Yu. Ivanov, and A. D. Bandrauk, 2011, Phys. Rev. A **83**, 013420.
Boot, H. A. H., S. A. Self, and R. B. R. Shersby-Harvie, 1958, J. Electron. Control **4**, 434.
Brabec, T., and F. Krausz, 2000, Rev. Mod. Phys. **72**, 545.
Brabec, T., M. Yu. Ivanov, and P. B. Corkum, 1996, Phys. Rev. A **54**, R2551.
Bucksbaum, P. H., M. Bashkansky, and T. J. McIlrath, 1987, Phys. Rev. Lett. **58**, 349.
Chen, J., J. H. Kim, and C. H. Nam, 2003, J. Phys. B **36**, 691.
Chen, J., J. Liu, L. B. Fu, and W. M. Zheng, 2000, Phys. Rev. A **63**, 011404(R).
Chen, J., J. Liu, and W. M. Zheng, 2002, Phys. Rev. A **66**, 043410.
Chen, J., and C. H. Nam, 2002, Phys. Rev. A **66**, 053415.
Chen, Z., Y. Liang, and C. D. Lin, 2010, Phys. Rev. Lett. **104**, 253201.
Chin, S. L., F. Yergeau, and P. Lavigne, 1985, J. Phys. B **18**, L213.
Corkum, P. B., 1993, Phys. Rev. Lett. **71**, 1994.
Corkum, P. B., 2011, Phys. Today **64**, No. 3, 36.
Cornaggia, C., and Ph. Hering, 1998, J. Phys. B **31**, L503.
Cornaggia, C., and Ph. Hering, 2000, Phys. Rev. A **62**, 023403.
Dammasch, M., M. Dörr, U. Eichmann, E. Lenz, and W. Sandner, 2001, Phys. Rev. A **64**, 061402(R).
de Jesus, V. L. B., B. Feuerstein, K. Zrost, D. Fischer, A. Rudenko, F. Afaneh, C. D. Schröter, R. Moshammer, and J. Ullrich, 2004, J. Phys. B **37**, L161.
de Jesus, V. L. B., A. Rudenko, B. Feuerstein, K. Zrost, C. D. Schröter, R. Moshammer, and J. Ullrich, 2004, J. Electron Spectrosc. Relat. Phenom. **141**, 127.
Delone, N. B., and V. P. Krainov, 1998, Phys. Usp. **41**, 469.
de Wijn, A. S., M. Lein, and S. Kuemmel, 2008, Europhys. Lett. **84**, 43 001.
Dietrich, P., N. H. Burnett, M. Ivanov, and P. B. Corkum, 1994, Phys. Rev. A **50**, R3585.
DiMauro, L. F., and P. Agostini, 1995, Adv. At. Mol. Opt. Phys. **35**, 79.
Dörner, R., V. Mergel, O. Jagutzki, L. Spielberger, J. Ullrich, R. Moshammer, and H. Schmidt-Böcking, 2000, Phys. Rep. **330**, 95.
Dörner, R., Th. Weber, M. Weckenbrock, A. Staudte, M. Hattas, H. Schmidt-Böcking, R. Moshammer, and J. Ullrich, 2002, Adv. At. Mol. Opt. Phys. **48**, 1.
Eberly, J. H., 1969, *Progress in Optics*, edited by E. Wolf (North-Holland, Amsterdam), Vol. VII, p. 361.
Eichmann, U., M. Dörr, H. Maeda, W. Becker, and W. Sandner, 2000, Phys. Rev. Lett. **84**, 3550.
Einstein, A., 1905, Ann. Phys. (Leipzig) **17**, 132.

Emmanouilidou, A., 2008, Phys. Rev. A **78**, 023411.
Eremina, E., X. Liu, H. Rottke, W. Sandner, M. G. Schätzel, A. Dreischuh, G. G. Paulus, H. Walther, R. Moshammer, and J. Ullrich, 2004, Phys. Rev. Lett. **92**, 173001.
Eremina, E., *et al.*, 2003, J. Phys. B **36**, 3269.
Faisal, F. H. M., 1973, J. Phys. B **6**, L312.
Faisal, F. H. M., 1987, *Theory of Multiphoton Processes* (Plenum Press, New York).
Faisal, F. H. M., 1994, Phys. Lett. A **187**, 180.
Faisal, F. H. M., and A. Becker, 1997, Laser Phys. **7**, 684.
Fedorov, M. V., 1997, *Atomic and Free Electrons in a Strong Light Field* (World Scientific, Singapore).
Feuerstein, B., *et al.*, 2001, Phys. Rev. Lett. **87**, 043003.
Figueira de Morisson Faria, C., 2009, J. Phys. B **42**, 105602.
Figueira de Morisson Faria, C., and W. Becker, 2003, Laser Phys. **13**, 1196.
Figueira de Morisson Faria, C., and M. Lewenstein, 2005, J. Phys. B **38**, 3251.
Figueira de Morisson Faria, C., and X. Liu, 2011, J. Mod. Opt. **58**, 1076.
Figueira de Morisson Faria, C., X. Liu, A. Sanpera, and M. Lewenstein, 2004, Phys. Rev. A **70**, 043406.
Figueira de Morisson Faria, C., X. Liu, H. Schomerus, and W. Becker, 2004, Phys. Rev. A **69**, 021402(R).
Figueira de Morisson Faria, C., H. Schomerus, X. Liu, and W. Becker, 2004, Phys. Rev. A **69**, 043405.
Figueira de Morisson Faria, C., T. Shaaran, X. Liu, and W. Yang, 2008, Phys. Rev. A **78**, 043407.
Fittinghoff, D. N., P. R. Bolton, B. Chang, and K. C. Kulander, 1992, Phys. Rev. Lett. **69**, 2642.
Forst, W., 1973, *Theory of Unimolecular Reactions* (Academic Press, New York).
Fu, L. B., J. Liu, J. Chen, and S. G. Chen, 2001, Phys. Rev. A **63**, 043416.
Fu, L. B., J. Liu, and S. G. Chen, 2002, Phys. Rev. A **65**, 021406(R).
Gillen, G. D., M. A. Walker, and L. D. Van Woerkom, 2001, Phys. Rev. A **64**, 043413.
Gingras, G., A. Tripathi, and B. Witzel, 2009, Phys. Rev. Lett. **103**, 173001.
Gontier, Y., and M. Trahin, 1989, J. Phys. B **22**, 2531.
Goreslavski, S. P., and S. V. Popruzhenko, 1996, Zh. Eksp. Teor. Fiz. **110**, 1200 [Sov. Phys. JETP **83**, 661 (1996)].
Goreslavski, S. P., and S. V. Popruzhenko, 2001, Opt. Express **8**, 395.
Goreslavskii, S. P., S. V. Popruzhenko, R. Kopold, and W. Becker, 2001, Phys. Rev. A **64**, 053402.
Greenman, L., P. J. Ho, S. Pabst, E. Kamarchik, D. A. Mazziotti, and R. Santra, 2010, Phys. Rev. A **82**, 023406.
Grobe, R., and J. H. Eberly, 1992, Phys. Rev. Lett. **68**, 2905.
Grobe, R., K. Rzążewski, and J. H. Eberly, 1994, J. Phys. B **27**, L503.
Gubbini, E., U. Eichmann, M. Kalashnikov, and W. Sandner, 2005a, Phys. Rev. Lett. **94**, 053602.
Gubbini, E., U. Eichmann, M. Kalashnikov, and W. Sandner, 2005b, J. Phys. B **38**, L87.
Guo, C., and G. N. Gibson, 2001, Phys. Rev. A **63**, 040701(R).
Guo, J., X.-S. Liu, and S.-I Chu, 2010, Phys. Rev. A **82**, 023402.
Haan, S. L., L. Breen, A. Karim, and J. H. Eberly, 2006, Phys. Rev. Lett. **97**, 103008.
Haan, S. L., N. Hoekema, S. Poniatowski, W.-C. Liu, and J. H. Eberly, 2000, Opt. Express **7**, 29.
Haan, S. L., and Z. S. Smith, 2007, Phys. Rev. A **76**, 053412.
Haan, S. L., Z. S. Smith, K. N. Shomsky, and P. W. Plantinga, 2008, J. Phys. B **41**, 211002.
Haan, S. L., Z. S. Smith, K. N. Shomsky, P. W. Plantinga, and T. L. Atallah, 2010, Phys. Rev. A **81**, 023409.
Haan, S. L., J. S. Van Dyke, and Z. S. Smith, 2008, Phys. Rev. Lett. **101**, 113001.
Haan, S. L., P. S. Wheeler, R. Panfili, and J. H. Eberly, 2002, Phys. Rev. A **66**, 061402(R).
Hagedorn, R., 1965, Nuovo Cimento Suppl. **3**, 147.
Hao, X. L., G. Q. Wang, X. Y. Jia, W. D. Li, J. Liu, and J. Chen, 2009, Phys. Rev. A **80**, 023408.
Hauge, E. H., and J. A. Støvneng, 1989, Rev. Mod. Phys. **61**, 917.
Herrwerth, O., *et al.*, 2008, New J. Phys. **10**, 025007.
Hertel, I. V., I. Shchatsinin, T. Laarmann, N. Zhavoronkov, H. H. Ritze, and C. P. Schulz, 2009, Phys. Rev. Lett. **102**, 023003.
Ho, P. J., 2007, Ph.D. thesis, University of Rochester.
Ho, P. J., and J. H. Eberly, 2003, Opt. Express **11**, 2826.
Ho, P. J., and J. H. Eberly, 2005, Phys. Rev. Lett. **95**, 193002.
Ho, P. J., and J. H. Eberly, 2006, Phys. Rev. Lett. **97**, 083001.
Ho, P. J., and J. H. Eberly, 2007, Opt. Express **15**, 1845.
Ho, P. J., X. Liu, and W. Becker, 2007, arXiv:physics/0703219.
Ho, P. J., R. Panfili, S. L. Haan, and J. H. Eberly, 2005, Phys. Rev. Lett. **94**, 093002.
Javanainen, J., J. H. Eberly, and Q. Su, 1988, Phys. Rev. A **38**, 3430.
Jia, X. Y., W. D. Li, J. Fan, J. Liu, and J. Chen, 2008, Phys. Rev. A **77**, 063407.
Jia, X. Y., W. D. Li, J. Liu, and J. Chen, 2009, Phys. Rev. A **80**, 053405.
Joachain, C. J., M. Dörr, and N. Kylstra, 2000, Adv. At. Mol. Opt. Phys. **42**, 225.
Johnson, N. G., *et al.*, 2011, Phys. Rev. A **83**, 013412.
Kaminski, P., R. Wiehle, W. Kamke, H. Helm, and B. Witzel, 2006, Phys. Rev. A **73**, 013413.
Kang, H., *et al.*, 2010, Phys. Rev. Lett. **104**, 203001.
Keldysh, L. V., 1964, Zh. Eksp. Teor. Fiz. **47**, 1945 [Sov. Phys. JETP **20**, 1307 (1965)].
Kibble, T. W. B., 1966, Phys. Rev. **150**, 1060.
Kondo, K., A. Sagisaka, T. Tamida, Y. Nabekawa, and S. Watanabe, 1993, Phys. Rev. A **48**, R2531.
Kopold, R., W. Becker, and M. Kleber, 2000, Opt. Commun. **179**, 39.
Kopold, R., W. Becker, H. Rottke, and W. Sandner, 2000, Phys. Rev. Lett. **85**, 3781.
Kopold, R., D. B. Milošević, and W. Becker, 2000, Phys. Rev. Lett. **84**, 3831.
Kornev, A. S., E. B. Tulenko, and B. A. Zon, 2009, Phys. Rev. A **79**, 063405.
Krausz, F., and M. Ivanov, 2009, Rev. Mod. Phys. **81**, 163.
Kuchiev, M. Yu., 1987, Pis'ma Zh. Eksp. Teor. Fiz. **45**, 319 [JETP Lett. **45**, 404 (1987)].
Kuchiev, M. Yu., 1995, J. Phys. B **28**, 5093.
Kuchiev, M. Yu., 1996, Phys. Lett. A **212**, 77.
Kulander, K. C., 1987, Phys. Rev. A **35**, 445.
Kulander, K. C., K. J. Schafer, and J. L. Krause, 1991, Int. J. Quantum Chem. Suppl. **25**, 415.
Kulander, K. C., K. J. Schafer, and J. L. Krause, 1992, in *Atoms in Intense Laser Fields*, edited by M. Gavrila (Academic Press, New York), p. 247, Sec. III.B.
Kulander, K. C., K. J. Schafer, and J. L. Krause, 1993, in *Super-Intense Laser-Atom Physics*, edited by B. Piraux, A. l'Huillier, and K. Rzążewski, NATO Advanced Studies Institute, Series B: Physics, Vol. 316 (Plenum, New York), p. 95.
Kurka, M., *et al.*, 2010, New J. Phys. **12**, 073035.
LaGattuta, K. J., and J. S. Cohen, 1998, J. Phys. B **31**, 5281.
Landau, L. D., and E. M. Lifishitz, 1977, *Quantum Mechanics* (Pergamon, Oxford).

Larochelle, S., A. Talebpour, and S. L. Chin, 1998, J. Phys. B **31**, 1201.
Lein, M., E. K. U. Gross, and V. Engel, 2000, Phys. Rev. Lett. **85**, 4707.
Lein, M., N. Hay, R. Velotta, J. P. Marangos, and P. L. Knight, 2002, Phys. Rev. A **66**, 023805.
Leopold, J. G., and I. M. Percival, 1978, Phys. Rev. Lett. **41**, 944.
Leopold, J. G., and I. M. Percival, 1979, J. Phys. B **12**, 709.
Lerner, P. B., K. J. LaGattuta, and J. S. Cohen, 1994, Phys. Rev. A **49**, R12.
Lerner, P. B., K. J. LaGattuta, and J. S. Cohen, 1996, J. Opt. Soc. Am. B **13**, 96.
Lewenstein, M., Ph. Balcou, M. Yu. Ivanov, A. L'Huillier, and P. B. Corkum, 1994, Phys. Rev. A **49**, 2117.
Lewenstein, M., K. C. Kulander, K. J. Schafer, and P. H. Bucksbaum, 1995, Phys. Rev. A **51**, 1495.
l'Huillier, A., L. A. Lompré, G. Mainfray, and C. Manus, 1983, Phys. Rev. A **27**, 2503.
Liu, J., D. F. Ye, J. Chen, and X. Liu, 2007, Phys. Rev. Lett. **99**, 013003.
Liu, W.-C., J. H. Eberly, S. L. Haan, and R. Grobe, 1999, Phys. Rev. Lett. **83**, 520.
Liu, X., and C. Figueira de Morisson Faria, 2004, Phys. Rev. Lett. **92**, 133006.
Liu, X., C. Figueira de Morisson Faria, and W. Becker, 2008, New J. Phys. **10**, 025010.
Liu, X., C. Figueira de Morisson Faria, W. Becker, and P. B. Corkum, 2006, J. Phys. B **39**, L305.
Liu, X., *et al.*, 2004, Phys. Rev. Lett. **93**, 263001.
Liu, Y., S. Tschuch, A. Rudenko, M. Dürr, M. Siegel, U. Morgner, R. Moshammer, and J. Ullrich, 2008, Phys. Rev. Lett. **101**, 053001.
Liu, Y., *et al.*, 2010, Phys. Rev. Lett. **104**, 173002.
Maeda, H., M. Dammasch, U. Eichmann, W. Sandner, A. Becker, and F. H. M. Faisal, 2000, Phys. Rev. A **62**, 035402.
Maharjan, C. M., A. S. Alnaser, X. M. Tong, B. Ulrich, P. Ranitovic, S. Ghimire, Z. Chang, I. V. Litvinyuk, and C. L. Cocke, 2005, Phys. Rev. A **72**, 041403(R).
Mainfray, G., and C. Manus, 1991, Rep. Prog. Phys. **54**, 1333.
Mauger, F., C. Chandre, and T. Uzer, 2009, Phys. Rev. Lett. **102**, 173002.
Mauger, F., C. Chandre, and T. Uzer, 2010a, Phys. Rev. Lett. **104**, 043005.
Mauger, F., C. Chandre, and T. Uzer, 2010b, Phys. Rev. Lett. **105**, 083002.
Milonni, P. W., M.-L. Shih, and J. R. Ackerhalt, *Chaos in Laser-Matter Interactions* (World Scientific, Singapore, 1987), Sec. 56.
Milošević, D. B., and W. Becker, 2003, Phys. Rev. A **68**, 065401.
Milošević, D. B., G. G. Paulus, D. Bauer, and W. Becker, 2006, J. Phys. B **39**, R203.
Moore, L. R., M. A. Lysaght, L. A. A. Nikolopoulos, J. S. Parker, H. W. van der Hart, and K. T. Taylor, 2011, J. Mod. Opt. **58**, 1132.
Moore, L. R., J. S. Parker, K. J. Meharg, G. S. J. Armstrong, and K. T. Taylor, 2008, J. Mod. Opt. **55**, 2541.
Morishita, T., A.-T. Le, Z. Chen, and C. D. Lin, 2008, Phys. Rev. Lett. **100**, 013903.
Moshammer, R., *et al.*, 2000, Phys. Rev. Lett. **84**, 447.
Moshammer, R., *et al.*, 2002, Phys. Rev. A **65**, 035401.
Moshammer, R., *et al.*, 2003, J. Phys. B **36**, L113.
Muth-Böhm, J., A. Becker, and F. H. M. Faisal, 2000, Phys. Rev. Lett. **85**, 2280.
Niikura, H., and P. B. Corkum, 2006, Adv. At. Mol. Opt. Phys. **54**, 511.
Niikura, H., F. Legare, R. Hasbani, A. D. Bandrauk, M. Yu Ivanov, D. M. Villeneuve, and P. B. Corkum, 2002, Nature (London) **417**, 917.
Nikolopoulos, L. A. A., J. S. Parker, and K. T. Taylor, 2008, Phys. Rev. A **78**, 063420.
Okunishi, M., R. Itaya, K. Shimada, G. Prümper, K. Ueda, M. Busuladžić, A. Gazibegović-Busuladžić, D. B. Milošević, and W. Becker, 2009, Phys. Rev. Lett. **103**, 043001.
Palacios, A., T. N. Rescigno, and C. W. McCurdy, 2009, Phys. Rev. A **79**, 033402.
Palaniyappan, S., A. DiChiara, E. Chowdhury, A. Falkowski, G. Ongadi, E. I. Huskins, and B. C. Walker, 2005, Phys. Rev. Lett. **94**, 243003.
Palaniyappan, S., I. Ghebregziabher, A. DiChiara, J. MacDonald, and B. C. Walker, 2006, Phys. Rev. A **74**, 033403.
Panfili, R., J. H. Eberly, and S. L. Haan, 2001, Opt. Express **8**, 431.
Panfili, R., S. L. Haan, and J. H. Eberly, 2002, Phys. Rev. Lett. **89**, 113001.
Panfili, R., and W.-C. Liu, 2003, Phys. Rev. A **67**, 043402.
Panfili, R., C. Szymanowski, W.-C. Liu, and J. H. Eberly, 2000, in *Multiphoton Processes: ICOMP VIII*, edited by L. F. Di Mauro, R. R. Freeman and K. C. Kulander (AIP Press, Woodbury, NY), p. 265.
Parker, J. S., B. J. S. Doherty, K. J. Meharg, and K. T. Taylor, 2003, J. Phys. B **36**, L393.
Parker, J. S., B. J. S. Doherty, K. T. Taylor, K. D. Schultz, C. I. Blaga, and L. F. DiMauro, 2006, Phys. Rev. Lett. **96**, 133001.
Parker, J. S., K. J. Meharg, G. A. McKenna, and K. T. Taylor, 2007, J. Phys. B **40**, 1729.
Parker, J. S., L. R. Moore, K. J. Meharg, D. Dundas, and K. T. Taylor, 2001, J. Phys. B **34**, L69.
Paulus, G. G., F. Grasbon, H. Walther, P. Villoresi, M. Nisoli, S. Stagira, E. priori, and S. De Silvestri, 2001, Nature (London) **414**, 182.
Paulus, G. G., F. Zacher, H. Walther, A. Lohr, W. Becker, and M. Kleber, 1998, Phys. Rev. Lett. **80**, 484.
Pazourek, R., J. Feist, S. Nagele, E. Persson, B. I. Schneider, L. A. Collins, and J. Burgdörfer, 2011, Phys. Rev. A **83**, 053418.
Perelomov, A. M., V. S. Popov, and M. V. Terentev, 1966, Zh. Eksp. Teor. Fiz. **50**, 1393 [Sov. Phys. JETP **23**, 924 (1966)].
Pfeiffer, A. N., C. Cirelli, M. Smolarski, R. Dörner, and U. Keller, 2011, Nature Phys. **7**, 428.
Pfeiffer, A. N., C. Cirelli, M. Smolarski, X. Wang, J. H. Eberly, R. Dörner, and U. Keller, 2011, New J. Phys. **13**, 093008.
Pohl, T., W. Ebeling, and M. Yu. Romanovsky, 2003, Phys. Lett. A **311**, 396.
Popov, A. M., O. V. Tikhonova, and E. A. Volkova, 2001, Opt. Express **8**, 441.
Popruzhenko, S. V., and S. P. Goreslavskii, 2001, J. Phys. B **34**, L239.
Popruzhenko, S. V., Ph. A. Korneev, S. P. Goreslavski, and W. Becker, 2002, Phys. Rev. Lett. **89**, 023001.
Prauzner-Bechcicki, J. S., K. Sacha, B. Eckhardt, and J. Zakrzewski, 2007, Phys. Rev. Lett. **98**, 203002.
Prauzner-Bechcicki, J. S., K. Sacha, B. Eckhardt, and J. Zakrzewski, 2008, Phys. Rev. A **78**, 013419.
Quan, W., X. Liu, and C. Figueira de Morisson Faria, 2009, J. Phys. B **42**, 134008.
Quan, W., *et al.*, 2009, Phys. Rev. Lett. **103**, 093001.
Reiss, H. R., 1962, J. Math. Phys. (N.Y.) **3**, 59.
Reiss, H. R., 1980, Phys. Rev. A **22**, 1786.
Reiss, H. R., 2008, Phys. Rev. Lett. **101**, 043002.

Rudenko, A., V. L. B. de Jesus, Th. Ergler, K. Zrost, B. Feuerstein, C. D. Schröter, R. Moshammer, and J. Ullrich, 2007, Phys. Rev. Lett. **99**, 263003.
Rudenko, A., K. Zrost, B. Feuerstein, V. L. B. de Jesus, C. D. Schröter, R. Moshammer, and J. Ullrich, 2004, Phys. Rev. Lett. **93**, 253001.
Ruiz, C., L. Plaja, and L. Roso, 2005, Phys. Rev. Lett. **94**, 063002.
Ruiz, C., L. Plaja, L. Roso, and A. Becker, 2006, Phys. Rev. Lett. **96**, 053001.
Sacha, K., and B. Eckhardt, 2001a, Phys. Rev. A **63**, 043414.
Sacha, K., and B. Eckhardt, 2001b, Phys. Rev. A **64**, 053401.
Salamin, Y. I., S. X. Hu, K. Z. Hatsagortsyan, and C. H. Keitel, 2006, Phys. Rep. **427**, 41.
Salières, P., *et al.*, 2001, Science **292**, 902.
Salières, P., A. l'Huillier, Ph. Antoine, and M. Lewenstein, 1999, Adv. At. Mol. Opt. Phys. **41**, 83.
Schafer, K. J., B. Yang, L. F. DiMauro, and K. C. Kulander, 1993, Phys. Rev. Lett. **70**, 1599.
Shaaran, T., C. Figueira de Morisson Faria, and H. Schomerus, 2011, arXiv:1107.3941.
Shaaran, T., M. T. Nygren, and C. Figueira de Morisson Faria, 2010, Phys. Rev. A **81**, 063413.
Shalashinin, D. V., M. S. Child, and A. Kirrander, 2008, Chem. Phys. **347**, 257.
Shvetsov-Shilovski, N. I., S. P. Goreslavski, S. V. Popruzhenko, and W. Becker, 2008, Phys. Rev. A **77**, 063405.
Smirnova, O., M. Spanner, and M. Yu. Ivanov, 2008, Phys. Rev. A **77**, 033407.
Smyth, E. S., J. S. Parker, and K. T. Taylor, 1998, Comput. Phys. Commun. **114**, 1.
Staudte, A., *et al.*, 2007, Phys. Rev. Lett. **99**, 263002.
Su, Q., and J. H. Eberly, 1991, Phys. Rev. A **44**, 5997.
Sukiasyan, S., C. McDonald, C. Van Vlack, C. Destefani, C. Varin, M. Ivanov, and T. Brabec, 2009, Chem. Phys. **366**, 37.
Taïeb, R., V. Véniard, and A. Maquet, 2001, Phys. Rev. Lett. **87**, 053002.
Talebpour, A., C.-Y. Chien, Y. Liang, S. Larochelle, and S. L. Chin, 1997, J. Phys. B **30**, 1721.
Talebpour, A., S. Larochelle, and S. L. Chin, 1997, J. Phys. B **30**, L245.
Ullrich, J., and V. Shevelko, 2003, Eds., *Many-Particle Quantum Dynamics in Atomic and Molecular Fragmentation*, Springer Series on Atomic, Optical, and Plasma Physics Vol. 35 (Springer, Berlin).
van der Hart, H. W., and K. Burnett, 2000, Phys. Rev. A **62**, 013407.
van Linden van den Heuvell, H. B., and H. G. Muller, 1988, in *Multiphoton Processes*, edited by S. J. Smith, and P. L. Knight, Cambridge Studies in Modern Optics Vol. 8 (Cambridge University Press, Cambridge, England), p. 25.
Walker, B., B. Sheehy, L. F. DiMauro, P. Agostini, K. J. Schafer, and K. C. Kulander, 1994, Phys. Rev. Lett. **73**, 1227.
Wang, X., and J. H. Eberly, 2011, arXiv:1102.0221.
Wang, X., and J. H. Eberly, 2009a, Laser Phys. **19**, 1518.
Wang, X., and J. H. Eberly, 2009b, Phys. Rev. Lett. **103**, 103007.
Wang, X., and J. H. Eberly, 2010a, Phys. Rev. Lett. **105**, 083001.
Wang, X., and J. H. Eberly, 2010b, New J. Phys. **12**, 093047.
Wasson, D. A., and S. E. Koonin, 1989, Phys. Rev. A **39**, 5676.
Watson, J. B., A. Sanpera, D. G. Lappas, P. L. Knight, and K. Burnett, 1997, Phys. Rev. Lett. **78**, 1884.
Weber, Th., H. Giessen, M. Weckenbrock, G. Urbasch, A. Staudte, L. Spielberger, O. Jagutzki, V. Mergel, M. Vollmer, and R. Dörner, 2000a, Nature (London) **405**, 658.
Weber, Th., *et al.*, 2000b, Phys. Rev. Lett. **84**, 443.
Weber, Th., *et al.*, 2000c, J. Phys. B **33**, L127.
Weckenbrock, M., A. Becker, A. Staudte, S. Kammer, M. Smolarski, V. R. Bhardwaj, D. M. Raymer, D. M. Villeneuve, P. B. Corkum, and R. Dörner, 2003, Phys. Rev. Lett. **91**, 123004.
Weckenbrock, M., M. Hattass, A. Czasch, O. Jagutzki, L. Schmidt, T. Weber, H. Roskos, T. Löffler, M. Thomson, and R. Dörner, 2001, J. Phys. B **34**, L449.
Weckenbrock, M., *et al.*, 2004, Phys. Rev. Lett. **92**, 213002.
Wolkow, D. M., 1935, Z. Phys. **94**, 250.
Xin, G. G., D. F. Ye, and J. Liu, 2010, Phys. Rev. A **82**, 063423.
Ye, D. F., and J. Liu, 2010, Phys. Rev. A **81**, 043402.
Ye, D. F., X. Liu, and J. Liu, 2008, Phys. Rev. Lett. **101**, 233003.
Yudin, G. L., and M. Yu. Ivanov, 2001a, Phys. Rev. A **63**, 033404.
Yudin, G. L., and M. Yu. Ivanov, 2001b, Phys. Rev. A **64**, 013409.
Zeidler, D., A. Staudte, A. B. Bardon, D. M. Villeneuve, R. Dörner, and P. B. Corkum, 2005, Phys. Rev. Lett. **95**, 203003.
Zon, B. A., 1999, JETP **89**, 219.
Zrost, K., A. Rudenko, Th. Ergler, B. Feuerstein, V. L. B. de Jesus, C. D. Schröter, R. Moshammer, and J. Ullrich, 2006, J. Phys. B **39**, S371.